Two-Dimensional Surface-Emitting Arrays of GaAs/AlGaAs Diode Lasers

J.P. Donnelly

Hybrid and monolithic two-dimensional surface-emitting arrays of GaAs/AlGaAs diode lasers have been designed and fabricated. The hybrid devices consist of linear arrays of edge-emitting graded-index separate-confinement-heterostructure single-quantum-well (GRIN-SCH-SQW) lasers mounted on a Si substrate containing integral 45° deflecting mirrors and microchannels for the flow of cooling fluid. With this design, CW output powers ≥120 W/cm^2 have been achieved. For quasi-CW operation (150-μsec pulses), peak output powers greater than 400 W/cm^2 appear to be achievable. Two types of monolithic arrays—the first of edge-emitting lasers with external-cavity deflecting mirrors adjacent to the laser facets and the second with intracavity 45° deflecting mirrors—have also been fabricated and tested.

Arrays of semiconductor diode lasers are of great interest for applications that require power levels higher than single devices can attain. Development efforts to date have concentrated mainly on linear arrays of edge-emitting GaAs/AlGaAs lasers [1–6]; these efforts have met with considerable success. Higher pulsed output power can be achieved by stacking and bonding these arrays to form composite two-dimensional arrays that are often referred to as rack-and-stack arrays [7–11]. Unless the stacking density is low, however, thermal considerations generally limit the maximum pulse repetition rate to less than 100 Hz.

An alternative to such composite arrays are monolithic two-dimensional arrays that consist of surface-emitting lasers. Several types of surface-emitting GaAs/AlGaAs and GaInAsP/InP diode lasers have been demonstrated, including lasers with resonant cavities that are normal to the surface (i.e., vertical-cavity lasers) [12–17], lasers that incorporate total-internal-reflecting 45° mirrors in the laser cavity [18–25], and lasers that utilize a second-order grating to achieve emission normal to the surface [26–29].

During the past several years, researchers have made substantial progress in developing all of the above monolithic surface-emitting techniques. In particular, although they still suffer from high series resistance and low power efficiency, vertical-cavity lasers that utilize epitaxially grown high-reflectivity quarter-wave stacks [30] to define the laser cavity have become an exciting area of research. Another approach to fabricating monolithic two-dimensional arrays is to couple edge-emitting diode lasers with external mirrors that deflect the radiation from the laser facets by 90° [21, 23, 31–39]. At Lincoln Laboratory, Z.L. Liau and J.N. Walpole [31–33] have fabricated such arrays of devices that combine a GaInAsP/InP laser with a parabolic deflector adjacent to one or both facets. The facets and deflectors are formed by selective chemical etching followed by a mass-transport process [31, 40, 41]. Because a similar mass-transport process is not available for AlGaAs, other techniques such as ion-beam-assisted etching (IBAE) [22, 42–45], modified IBAE [46, 47], reactive ion etching [22, 24, 48], and ion milling [24, 35, 36] have been used to form the noncleaved laser facets and adjacent deflecting mirrors. Although these monolithic techniques hold great promise for the high-volume production of large-area high-power laser arrays, they are still in the early stages of development.

This article will discuss several approaches to fabricating two-dimensional surface-emitting arrays of GaAs/AlGaAs diode lasers:

- a hybrid approach [21, 49, 50] in which linear arrays of edge-emitting lasers with cleaved end facets are mounted on microchannel Si heat sinks that have integral 45° deflecting mirrors,
- a monolithic approach in which edge-emitting lasers are fabricated such that the deflecting mirrors are adjacent to both of the end facets of each laser, and
- a monolithic approach in which horizontal-cavity lasers with intracavity 45° deflecting mirrors are fabricated.

In both monolithic approaches, all the laser facets and deflecting mirrors are fabricated by IBAE. The hybrid approach is a technology that can be implemented today. In fact, arrays made with this process are currently being used to side-pump Nd:YAG slab lasers. Much of the packaging and heat-sink technology being developed for hybrid arrays should be applicable to monolithic arrays, which are considered to be a more long-term technology than the hybrid arrays. It is important to note that the two-dimensional output patterns of monolithic arrays are determined photolithographically. Thus it should be easier to integrate these arrays with arrays of lenses for increased pump intensity or for incorporation in external cavities to combine individual elements coherently [51, 52].

Hybrid Surface-Emitting Arrays

Figure 1 is a schematic illustration of a hybrid two-dimensional surface-emitting array [21, 49, 50]. The device consists of linear arrays of edge-emitting lasers with conventional cleaved end facets mounted in grooves with flat bottoms and 45° sidewalls etched in a Si substrate. The substrate contains microchannels [53–60] for the flow of cooling fluid; the microchannel cooling provides an efficient means of removing high average dissipated powers. The Cu bar on top of each linear array provides high electrical conductivity along the array and transient heat sinking during pulsed operation. This section first discusses the AlGaAs epitaxial material from which the linear arrays are fabricated. Next, the fabrication and performance of the linear arrays and the microchannel Si heat sinks are discussed.

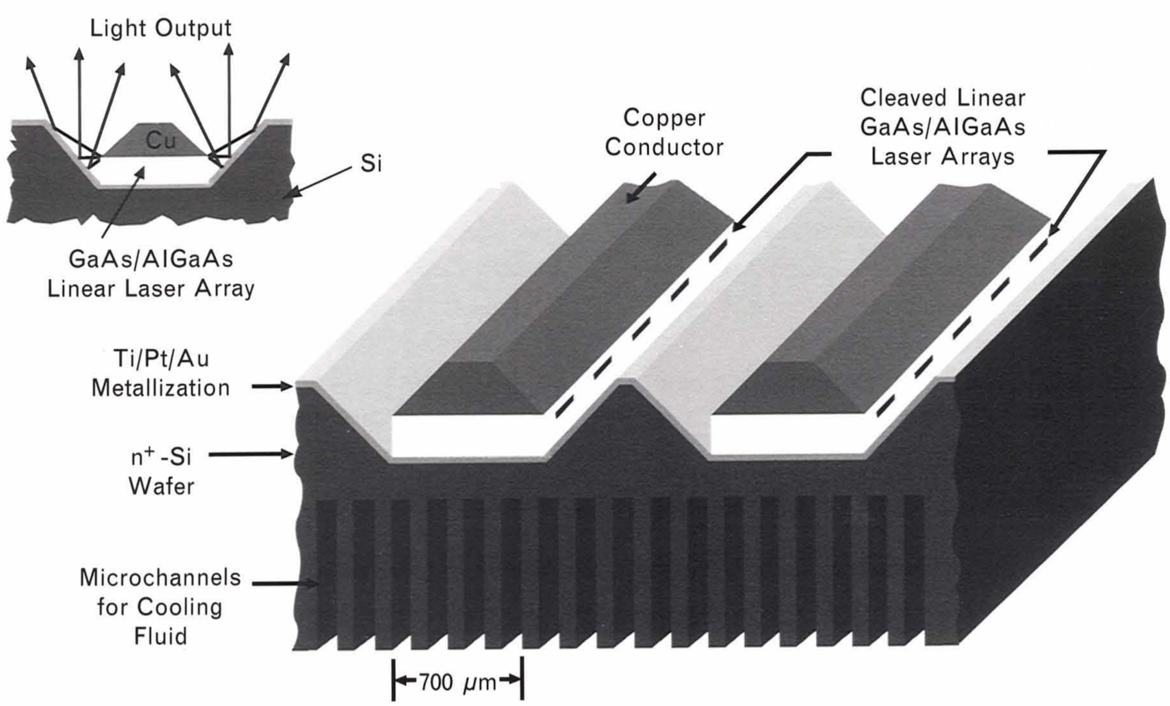

FIGURE 1. Schematic diagram of a hybrid two-dimensional surface-emitting array of GaAs/AlGaAs diode lasers with integral Si heat sink.

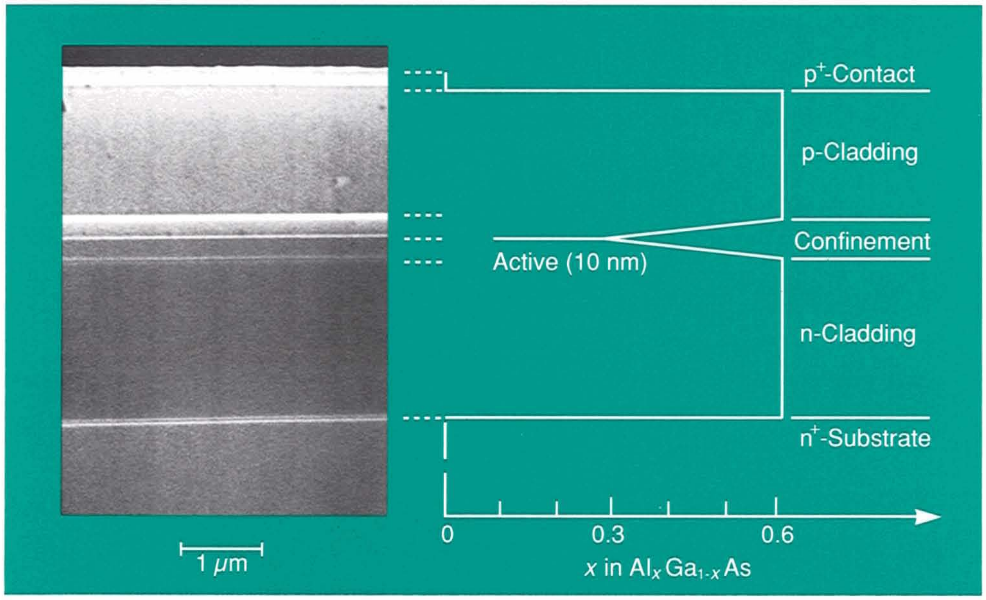

FIGURE 2. Scanning-electron micrograph of the graded-index separate-confinement-heterostructure single-quantum-well (GRIN-SCH-SQW) laser structure with layer identification on right.

Performance data on modules containing two 1-cm^2 hybrid arrays are then presented and discussed.

Material

In order to fabricate high-efficiency high-power arrays, we must reproducibly grow uniform laser material with low threshold current density J_{th}, high differential quantum efficiency η_d, and low series resistance R_s. For many applications, such as the pumping of Nd:YAG lasers for which the emission wavelength including any chirping during pulsed operation must be between 804 and 810 nm, we must also reproducibly control the emission wavelength of the diode laser material.

The linear arrays used in the two-dimensional hybrid arrays are fabricated in AlGaAs material with a graded-index separate-confinement-heterostructure single-quantum-well (GRIN-SCH-SQW) structure (Figure 2). The GRIN-SCH-SQW structure is grown on n^+-GaAs by organometallic vapor phase epitaxy (OMVPE). The quantum well is typically 100 Å thick and contains ~7 mole % AlAs. The GRIN region on either side of the quantum well is graded from 30 to 60 mole % AlAs over approximately 2000 Å, which makes the confinement region approximately 4100 Å thick. Extensive development of Lincoln Laboratory's OMVPE reactor has yielded uniform precision growth of the desired laser structure and lasers with low J_{th} and high η_d [61]. Some of the important design features of the reactor include a vertical growth chamber, porous-plug gas injection, low-pressure (0.2 atm) operation, and high substrate rotation rates. Reference 62 contains details of the reactor development.

We evaluated the uniformity of material grown in the reactor by randomly selecting a laser wafer and testing lasers fabricated from different sections of the wafer. For 192 broad-area lasers with 500-μm cavity lengths taken from different sections of a 2-in wafer, the mean value of J_{th} was 287.5 A/cm^2 with a standard deviation of 11.3 A/cm^2 [61, 62]. The mean value of η_d was 83% with a standard deviation of 2.5%. The highest value of η_d was 88%, which is among the highest reported in the literature. The mean value and standard deviation of the emission wavelength were 804.9 nm and 0.6 nm, respectively. The mean value of emission wavelength for 10 different wafers ranged from 803.5 to 807.4 nm, and wafer-to-wafer variations in J_{th} and η_d were typically less than 10%.

Figure 3 plots the values of J_{th} and η_d^{-1} versus cavity length for broad-area lasers fabricated from a typical wafer. The value of J_{th} decreases with cavity length and is typically 200 A/cm^2 for a length of 700 μm, the cavity length used in the hybrid arrays. From the plot of η_d^{-1}, the internal absorption coefficient α in the GRIN-SCH-SQW material tested was determined to be ~2.5 cm^{-1}

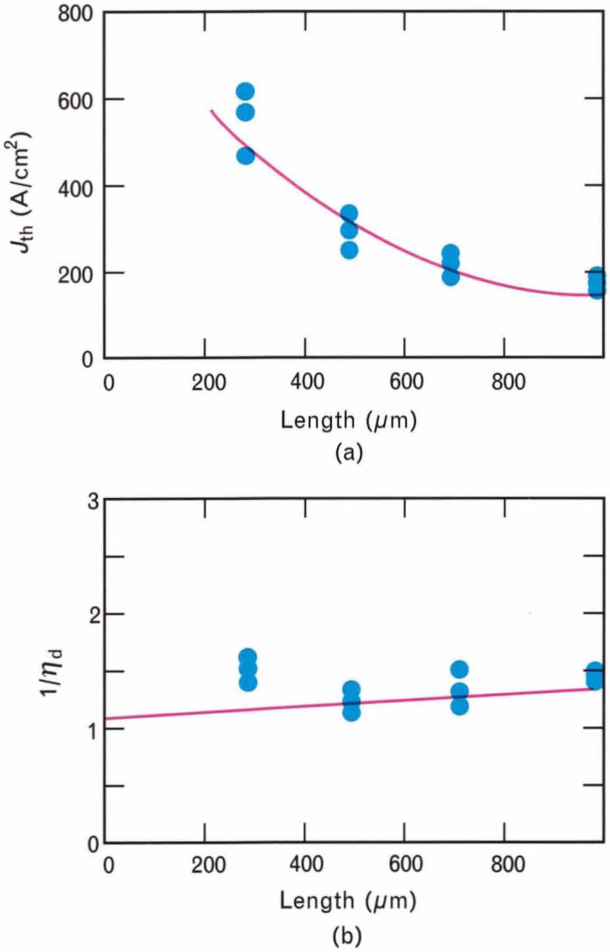

FIGURE 3. (a) Threshold current density J_{th} and (b) reciprocal of differential quantum efficiency η_d^{-1} versus cavity length for broad-area GRIN-SCH-SQW diode lasers.

[61]. This low internal loss is responsible for the low J_{th} and high external η_d obtained even on lasers with long cavity lengths.

Because J_{th}, and therefore the population inversion in the 100-Å quantum wells, changes with cavity length, the emission wavelength also changes. Facet coatings, which are used to prevent facet degradation, can also affect the wavelength through changes in facet reflectivity and, consequently, in J_{th}. Figure 4 illustrates how the emission wavelength changes with J_{th} in these lasers. Note that a 15% change in J_{th} around a value of 200 A/cm^2 results in about a 1-nm shift in lasing wavelength.

As mentioned previously, in addition to low J_{th} and high η_d, low R_s is important to obtain a laser that has high power efficiency and a minimum increase in temperature during high-power operation. (Large increases in temperature degrade both laser performance and lifetime, and contribute to chirping of the laser wavelength during pulsed operation.) Figure 5 illustrates that lasers fabricated in material with abrupt heterojunctions between the top p$^+$-GaAs contacting layer and p$^-$-AlGaAs cladding layer, and between the n$^-$-AlGaAs cladding layer and n$^+$-GaAs substrate, exhibit large nonlinear series resistances. Compositionally grading these interfaces reduces the height of these parasitic heterojunction barriers [63, 64], and enables the fabrication of laser diodes with low R_s. The value of R_s for 40 × 700-μm laser diodes with graded p$^+$/p$^-$ and n$^-$/n$^+$ heterojunctions is typically less than 0.2 Ω.

Linear Arrays

For use in the two-dimensional hybrid arrays, linear arrays of proton-defined stripe lasers (Figure 6) have been fabricated in the GRIN-SCH-SQW AlGaAs material. Following the deposition of a top ohmic contact, a shallow proton bombardment that penetrates to a depth approximately 0.2 μm above the top GRIN region converts the bombarded regions to high-resistivity material [65, 66], thus confining current to the nonbombarded laser stripes. A second proton bombardment at higher energies into 10-μm stripes midway between the laser stripes introduces sufficient optical loss to suppress lasing in the transverse direction. After the

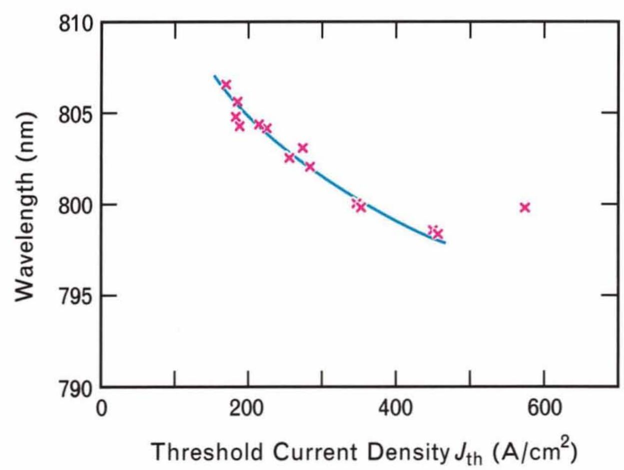

FIGURE 4. Emission wavelength versus threshold current density of diode lasers fabricated from a typical AlGaAs GRIN-SCH-SQW wafer in which the quantum-well thickness is 100 Å. Changes in the threshold current density result from changes in cavity length and facet reflectivity.

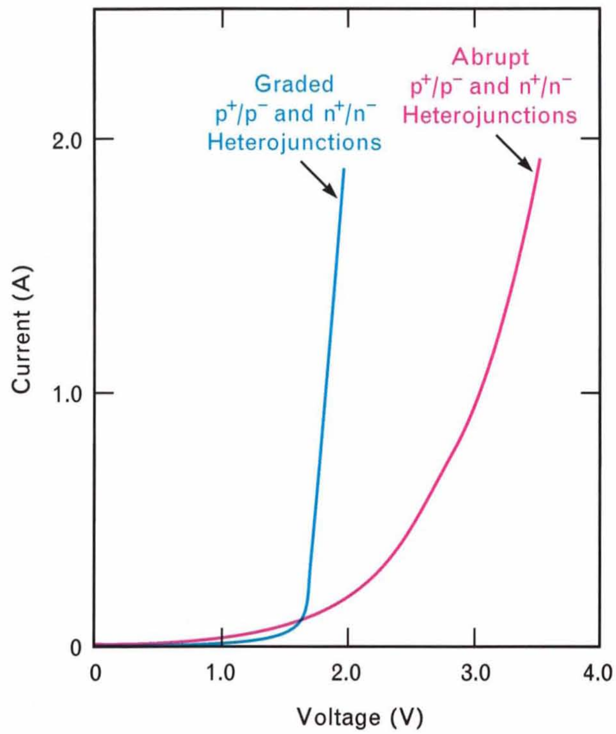

FIGURE 5. Typical current-voltage characteristics of 40 × 700-μm GRIN-SCH-SQW lasers with abrupt p^+-GaAs/p^--$Al_{0.6}Ga_{0.4}As$ and n^--$Al_{0.6}Ga_{0.4}As$/n^+-GaAs-substrate contacting heterojunctions, and with graded contacting heterojunctions. With graded heterojunctions, the series resistance for this size laser is less than 0.2 Ω.

wafers are thinned to ~100 μm and ohmic contacts made to the n^+-GaAs substrate, linear arrays of the appropriate length are cleaved from the wafers and the facets coated with approximately a half-wavelength-thick layer of Al_2O_3.

The performance of the linear arrays depends on the stripe width W and laser period S. Figure 7 plots J_{th} and emission wavelength for proton-defined uncoated lasers made from 800-nm material versus W. For stripes wider than ~40 μm, the values of J_{th}, emission wavelength, and η_d (not shown) are nearly constant. Below 40 μm, J_{th} increases with a corresponding decrease in emission wavelength and η_d. In addition, for 10 μm < W < 40 μm, kinks are observed in the light-output-versus-current (L-I) characteristics and the emission spectrum is not well behaved with drive current; i.e., blue-shifted, or higher-energy, modes begin to appear as the drive current increases and the spectrum can become very broad and fairly complicated. For narrow stripes ($W \leq 10$ μm), the L-I characteristics and emission are again well behaved. For these narrow widths, however, J_{th} is significantly higher and η_d significantly lower than the values obtained on broad-area lasers. In fact, for $W = 5$ μm, J_{th} increases to the extent that the lasing wavelength jumps to a transition between higher-energy quantum-well levels. Thus we have used stripes at least 40 μm wide in the linear arrays.

As previously discussed, facet coatings that decrease reflectivity also increase the threshold current, and blue-shift the emission spectrum. For coatings ~15% thicker than $\lambda/2$, where λ is the laser wavelength, the value of J_{th} for the lasers with $W \geq 40$ μm increases by ~30 A/cm^2 (an increase of 15%), and the laser wavelength decreases to ~799 nm. For pumping Nd:YAG, therefore, control of the facet-coating thickness does not appear to be critical and tolerances as large as ±15% should be acceptable.

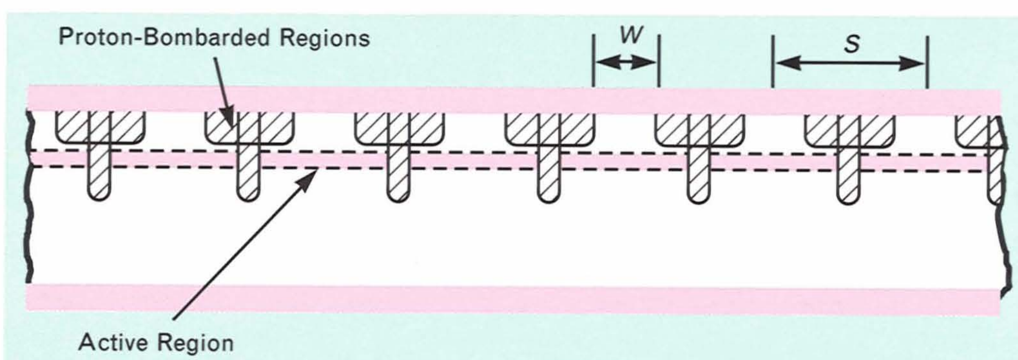

FIGURE 6. Illustration of proton-defined linear array of AlGaAs GRIN-SCH-SQW lasers. A shallow proton bombardment confines the current to unbombarded stripes of width W and a deep proton bombardment suppresses lasing in the transverse direction.

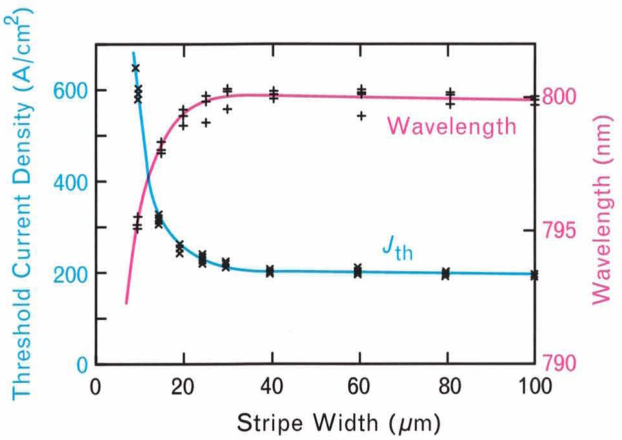

FIGURE 7. Threshold current density J_{th} and peak emission wavelength versus stripe width for proton-defined AlGaAs GRIN-SCH-SQW stripe diode lasers. The lasers have uncoated facets and cavity lengths of 700 μm.

Once J_{th} and η_d versus W are known, the temperature rise ΔT in the middle of each laser stripe, the power efficiency η_p, and the required operating current I_{op} can be calculated for any values of W, S, pulse length, and desired output power. Because the wavelength of AlGaAs lasers increases by approximately 0.3 nm per 1°C rise in temperature, the temperature rise must be kept as small as possible to minimize wavelength chirping during pulsed operation—an important consideration for applications such as the pumping of Nd:YAG lasers in which the emission wavelength must remain in the Nd:YAG absorption band during the entire pulse. In addition, because J_{th} increases and η_d decreases with increasing temperature (although the rate of change is small for AlGaAs quantum-well lasers), minimizing the temperature rise ΔT to prevent degradation of the overall laser performance is desirable.

As an example of the kind of performance that can be expected, Figure 8 shows I_{op}, η_p, and ΔT as functions of S for a linear array with W = 40 μm and a fixed output power of 30 W during a single 150-μsec pulse. A value of 150 μsec was used because it is a reasonable pulse length for the pumping of Nd:YAG, which has an excited Nd lifetime of ~230 μsec. A 1-cm-long linear array mounted junction side up was assumed. Two-dimensional transient heat flow was used in calculating ΔT; the calculations were performed both including [67] and neglecting transient heat flow into the top Cu conducting bar (Figure 1). The presence of the Cu bars, as shown in Figure 8, significantly reduced the transient ΔT and, in addition, acted as a heat spreader, making ΔT less sensitive to the laser period S [67]. Also note that there are trade-offs between ΔT, η_p, and I_{op}. For the stripe width and output power of Figure 8, a value of S between 100 and 150 μm appears to be a good compromise for most applications. For lower peak

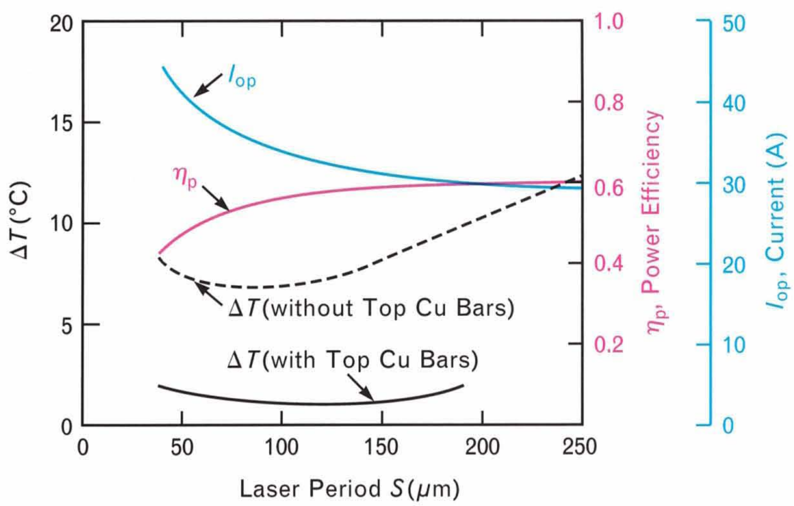

FIGURE 8. Calculated operating parameters of a 1-cm-long proton-defined AlGaAs GRIN-SCH-SQW linear diode laser array with 40-μm-wide laser stripes: the calculated temperature rise ΔT in the center of each laser stripe with and without the top Cu conducting bars, the power efficiency η_p, and required operating current I_{op} versus laser period S. The data are for a cavity length of 700 μm, a fixed output power of 30 W during a single 150-μsec pulse, and the worst-case J_{th} and R_s.

output powers a larger S may be warranted, and for higher peak output powers a smaller S. Calculations indicate, however, that even for a higher output of 50 W during a 150-μsec pulse, the maximum transient ΔT should be less than 2°C for S between 100 and 150 μm.

The calculated temperature rise in Figure 8 is for a single 150-μsec pulse. Higher repetition rates shift the ΔT curve up by approximately the average temperature rise that results from the average power dissipation. Microchannel Si heat sinks are very effective in removing high average power dissipation.

Microchannel Si Heat Sinks

The flat-bottom grooves with 45° sidewalls in the heat sink in which the laser bars are mounted (Figure 1) are etched in (100) silicon with standard photolithography and an orientation-selective etch. A stripe pattern oriented in an (013) direction is first defined in a Si_3N_4 capping layer that serves as an etch mask. The Si is then etched with a KOH-isopropanol-H_2O solution at 80°C. The bottom (100) Si plane etches about 2.5 times faster than the (331) sidewalls. Figure 9(a) shows a sawed cross section of a test etched groove. Because the etch ratio is only 2.5, the actual angles between the sidewalls and the top and bottom are closer to 45° than the theoretical angle of 46.5° between the (331) and (100) planes. After etching, the surface of the Si is metallized with Ti/Pt/Au to form efficient deflecting mirrors. Figure 9(b) shows a top view of a metallized test Si sample with a GaAs/AlGaAs linear array mounted in a groove. Reflections of the cleaved end facets of the GaAs/AlGaAs bar are clearly visible in the 45° deflecting mirrors. For the actual hybrid arrays reported here, the etched grooves were about 210 μm deep with 700-μm-wide bottoms.

We used a dicing saw to cut microchannels into the bottom of the Si heat sink [58, 60]. Figure 10, a photomicrograph of the sawed cross section of a portion of an actual hybrid array, shows a linear array mounted in an etched groove in a microchannel Si heat sink. The sawed microchannels are 100 μm wide and spaced every 200 μm. The top Cu conductor is tapered so that it will not block any of the light that emerges from the surface of the array.

Theoretical calculations [55–57] and experimental results [58, 60] indicate that with a reasonable cooling-fluid pump power (~10 W for a 1 × 1-cm array), the microchannel Si heat sinks will have a CW thermal resistance of less than 0.07°C-cm^2/W (at the top surface

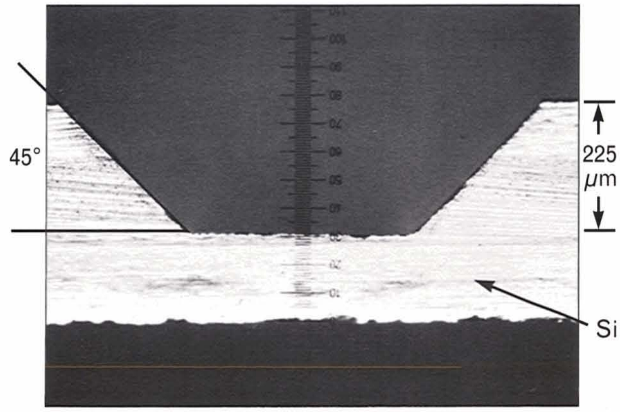

(a)

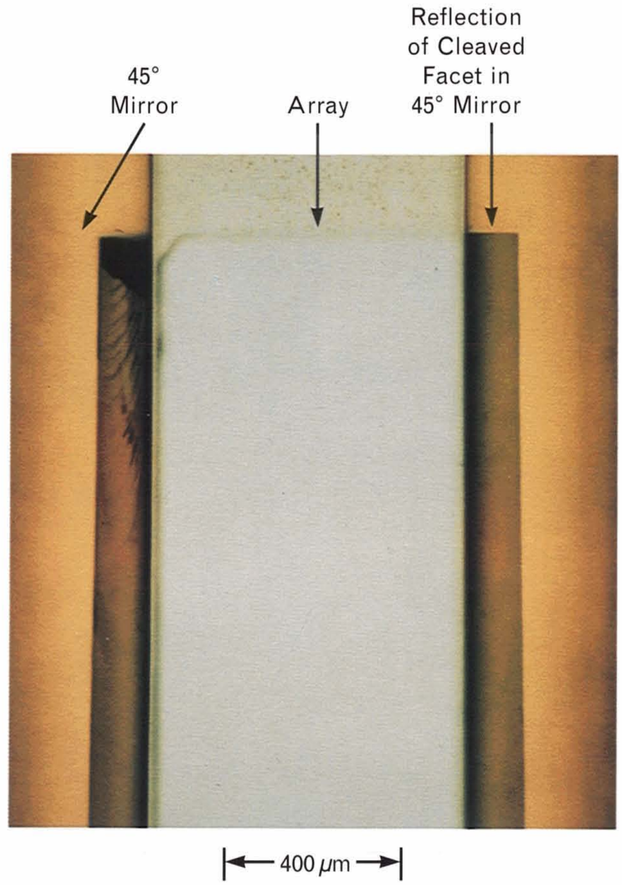

(b)

FIGURE 9. Etched groove in Si heat sink: (a) sawed cross section of flat-bottom test groove with 45° sidewalls and (b) top view of GaAs/AlGaAs linear array mounted in the metallized groove. Reflections of cleaved end facets of the linear array can be seen in the 45° mirrors.

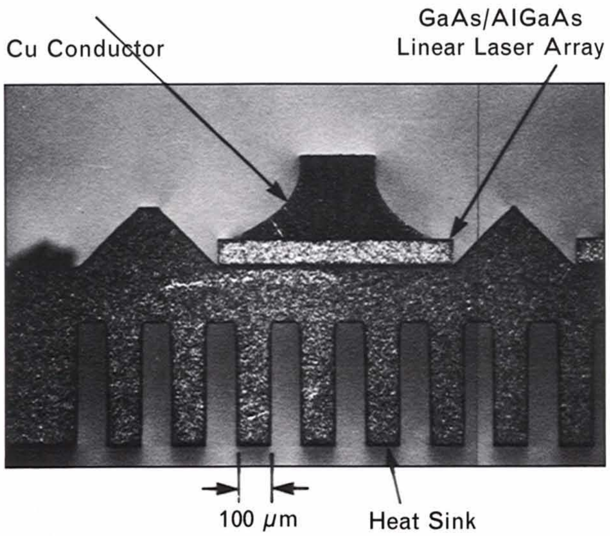

FIGURE 10. Sawed cross section of an actual hybrid GaAs/AlGaAs diode laser array showing the end of one linear array mounted in an etched groove in a microchannel Si heat sink. The top Cu conductor is tapered so that it will not block any light that emerges from the surface of the array.

of the Si heat sink) and that the microchannels themselves can be treated as having an effective heat transfer coefficient $h_{eff} \geq 20$ W/cm^2-°C. The hybrid devices reported here have their linear laser arrays mounted junction side up, which adds to the CW thermal resistance.

Figure 11 shows the transient ΔT per unit power dissipation (during each pulse) at the beginning of a 150-μsec, 400-Hz pulse train for an AlGaAs laser bar mounted junction side up on a Si heat sink. Figure 11(a) is for the case in which the top Cu conducting bars are neglected and Figure 11(b) is for the case in which the Cu bars are included in the calculation [67]. The figures assume that the GaAs is 100 μm thick and the Si heat sink has 150 μm of Si above the microchannels. The calculation is for uniform power dissipation on top of the GaAs. For 40-μm-wide stripe lasers on 125-μm centers, the maximum temperature rise in the center of each laser stripe at the end of each pulse is about 9×10^{-3}°C-cm^2/W higher than the values shown in Figure 11(a) and about 1.5×10^{-3}°C-cm^2/W higher than the values shown in Figure 11(b).

Figure 11 demonstrates the benefits of the microchannel heat sinks. Without the top Cu bars, it only takes three to four pulses at this high repetition rate before the temperature transient during each pulse no longer changes from pulse to pulse. In this case, the maximum peak temperature difference between the first pulse and a steady-state pulse is only about 2×10^{-3}°C-cm^2/W. For a linear array emitting 30 W of optical power, this difference translates into an additional temperature rise of ~0.6°C at the peak of each pulse as the repetition rate increases from essentially isolated pulses to 400 Hz.

When the top Cu bars are included in the thermal analyses, they act as large thermal capacitors, damping the peak temperature excursions to approximately 3×10^{-3}°C-cm^2/W but slowing down the thermal time constant of the system. In this case, it takes about 10 pulses (100 msec) before the temperature transient during each pulse no longer changes from pulse to pulse and the maximum temperature difference between

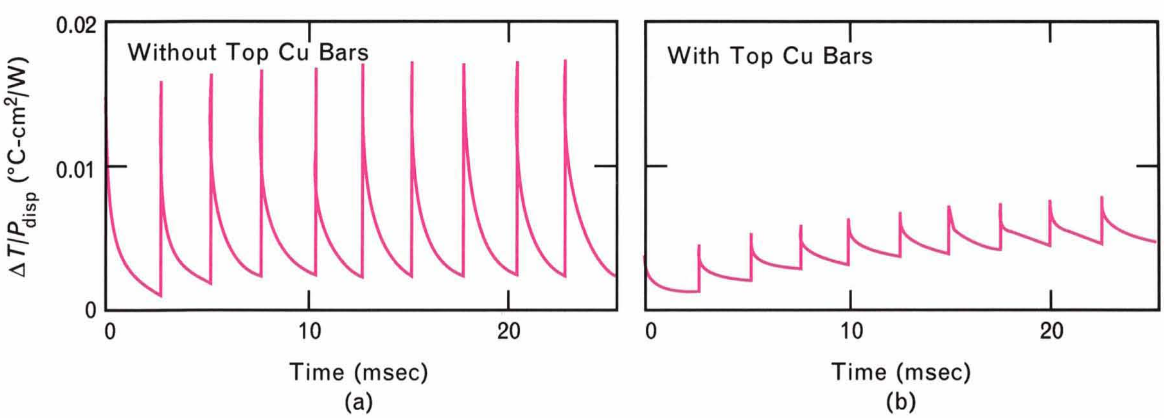

FIGURE 11. The normalized calculated temperature transient on the top of a 100-μm-thick GaAs laser bar at the start of a 150-μsec 400-Hz pulse train: (a) without the top Cu conducting bars, and (b) with the top Cu conducting bars. The laser bar is mounted junction side up on a microchannel Si heat sink. (After J.N. Walpole, Reference 67.)

(a)

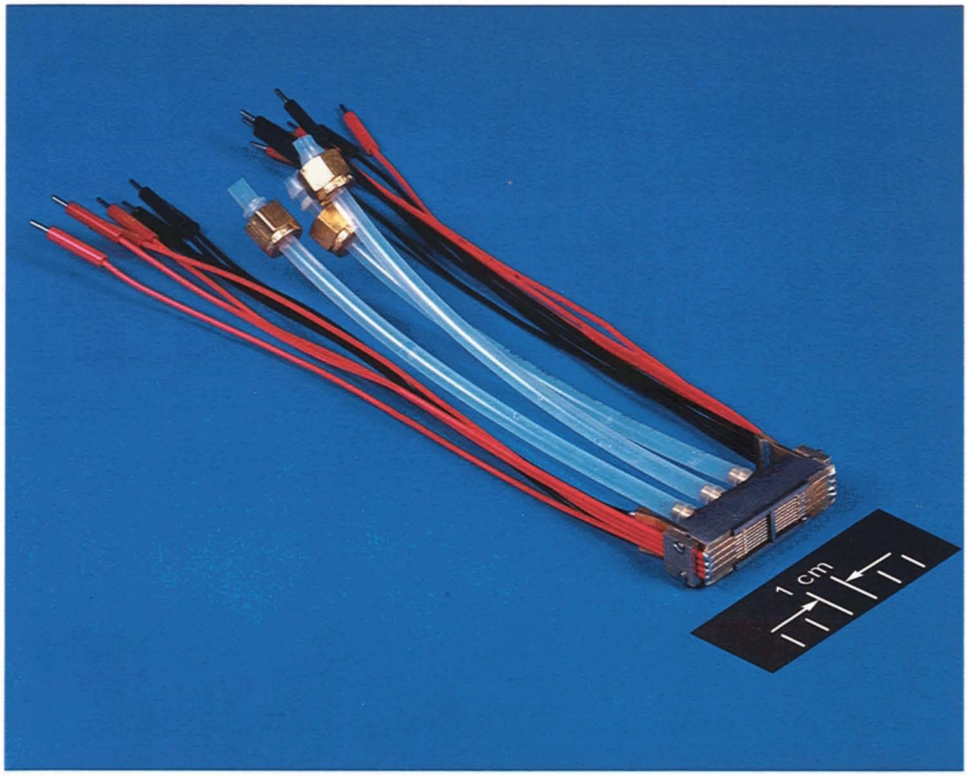

(b)

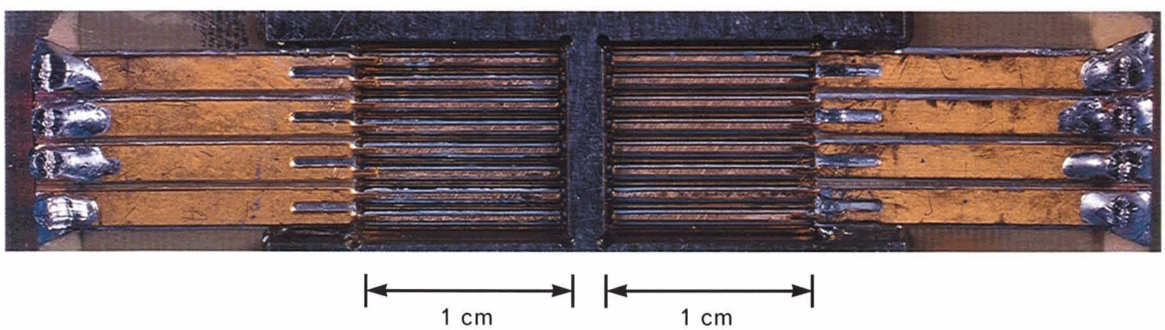

FIGURE 12. Completed module that contains two 1-cm^2 two-dimensional surface-emitting arrays of diode lasers: (a) overall view and (b) view of front face.

the peak of a first pulse and the peak of a steady-state pulse is ~4.5×10^{-3}°C-cm^2/W. For a 1-cm linear laser array emitting 30 W of optical power, this difference translates into an additional temperature rise of ~1.38°C as the repetition rate increases from essentially isolated pulses to 400 Hz. Note, however, that the transient temperature during each pulse is now only ~1.3°C for the 30-W scenario compared to ~7°C without the top Cu bars (Figure 8).

For uniform heat dissipation across the laser bar, the average temperature rise is the same both with and without the Cu bars. For CW operation, the only effect of the top Cu bars is to act as heat spreaders, a secondary but important consideration that makes the temperature across the top of the laser bar more uniform and less dependent on the laser width W and spacing S.

Hybrid-Array Performance

Figure 12 shows photographs of a completed laser module that contains two 1-cm^2 hybrid arrays, each of which consists of eight 1-cm-long linear arrays soldered in eight grooves on a microchannel Si heat sink. In this design, the linear arrays are driven in pairs. Cooling fluid enters the module through a center tube and

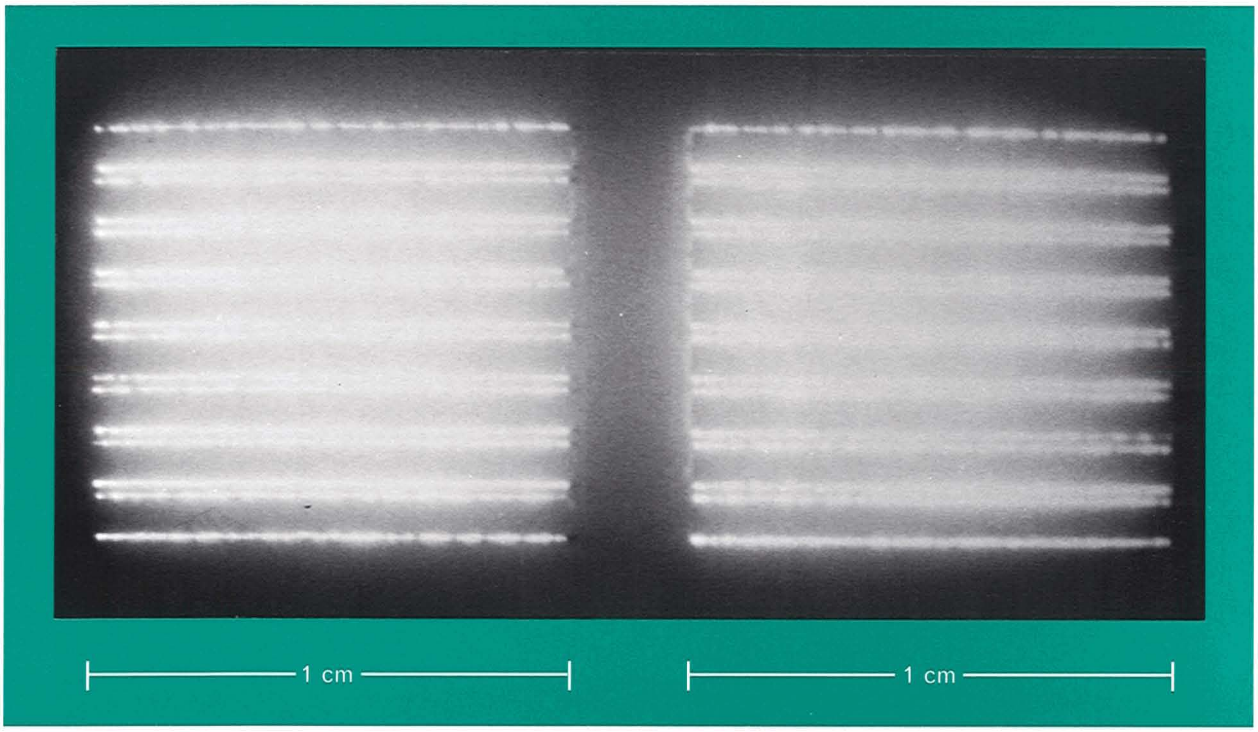

FIGURE 13. Near-field pattern of a module that contains two 1-cm^2 surface-emitting hybrid AlGaAs GRIN-SCH-SQW diode laser arrays.

exits through two outside tubes.

Figure 13 shows the near-field pattern of a completed module. The geometry of these hybrid arrays is such that the amount of thermal cross talk between the individual linear arrays is insignificant. Thus testing the linear-array bars individually or in pairs one pair at a time provides a good idea of the ultimate performance of the hybrid arrays.

Figure 14 shows the output power versus current (L-I characteristic) of successive pairs of laser bars in a module driven with 150-μsec current pulses at 10 Hz. Note that the response is very uniform with high η_d

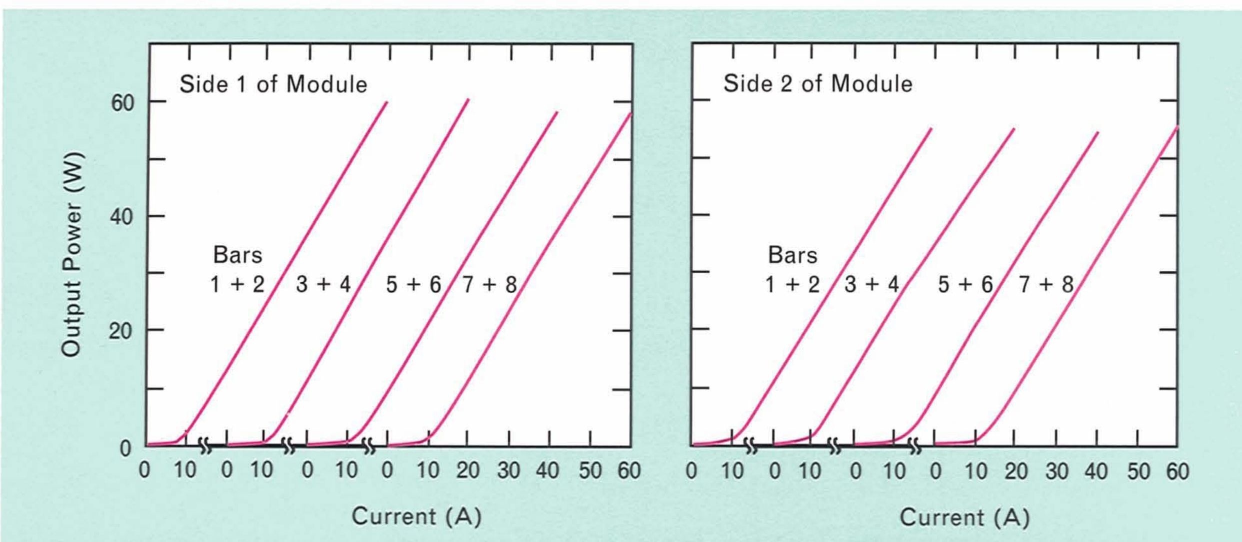

FIGURE 14. Pulsed output power versus current for 150-μsec pulses at 10 Hz into successive pairs of laser bars of a module that contains two 1-cm^2 two-dimensional surface-emitting hybrid arrays of AlGaAs diode lasers.

for all pairs in the array. From these data, the total energy per 150-μsec pulse from the entire module with 60 A through each pair (30 A per 1-cm-long linear array) should be 68 mJ. Separate measurements using a calorimeter with the entire module driven at one time have given a total energy of 64 mJ per pulse [68].

Figure 15 shows the L-I characteristics of a pair of laser bars driven with 150-μsec pulsed currents up to 100 A. From these data, we estimate that if the entire module were driven with 100 A per pair (50 A per bar), the output energy per pulse would be ~120 mJ. Figure 16 shows the integrated output spectra of the laser pair driven with 40-A (20 A/bar) and 80-A (40 A/bar) 150-μsec pulses at 10 Hz. The spectra are typical of most arrays.

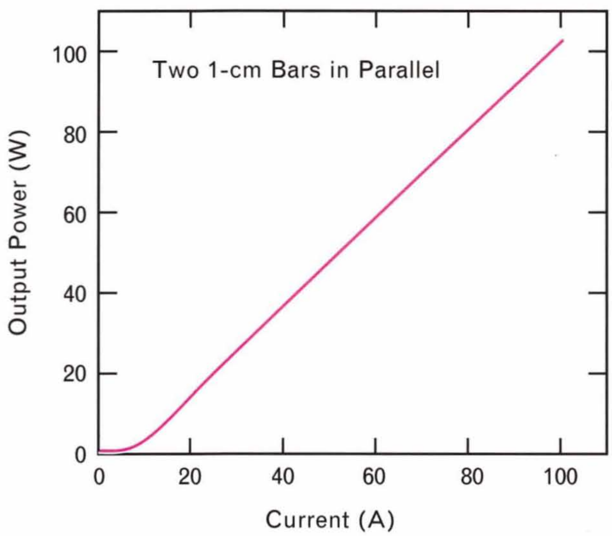

FIGURE 15. Pulsed output power versus current of a single pair of parallel 1-cm laser bars of a hybrid array driven with 150-μsec pulses at 10 Hz.

Additional tests were performed by disconnecting one bar of several pairs and then testing the remaining bars individually at various currents, pulse widths, and repetition rates. Figure 17 shows the L-I characteristics of one 1-cm-long bar of a hybrid array driven with 150-μsec pulses at repetition rates up to 500 Hz. The lasers in the array were 40 μm wide and spaced on center at 125 μm. Note that at 40 A, there was less than a 10% decrease in output per pulse at 500 Hz compared with that at 10 Hz.

We also obtained the output spectra of the same bar

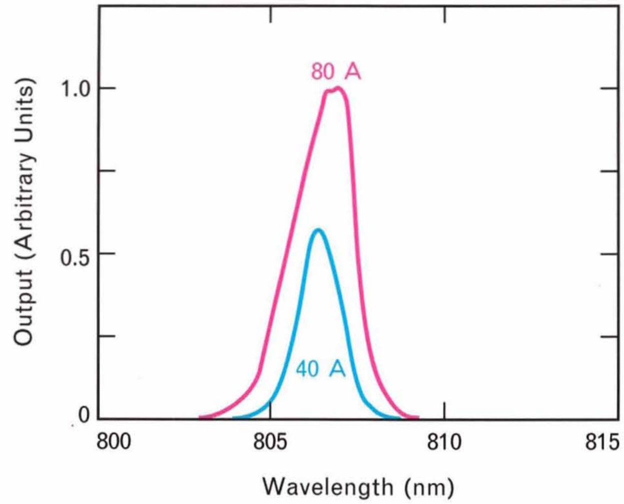

FIGURE 16. Output spectra of a pair of parallel 1-cm-long bars of GRIN-SCH-SQW lasers (40 μm wide on 125-μm centers) of a hybrid array. The bars were driven with 40-A (20 A/bar) and 80-A (40 A/bar) 150-µsec pulses at 10 Hz.

driven with 150-μsec pulses at various currents up to 30 A at 10 Hz, and with 150-μsec pulses of 30 A at repetition rates from 10 to 500 Hz. At the higher currents, the output of the particular bar tested showed anomalous blue-shifted modes, which are not usually observed. The wavelength change at 30 A compared with that at 7 A indicated a temperature rise of <3°C during a 30-A 150-μsec pulse. (As mentioned previously, the wavelength of AlGaAs lasers increases by ~0.3 nm

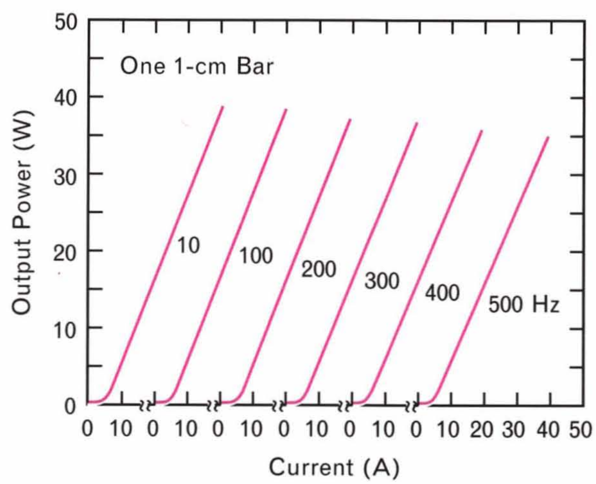

FIGURE 17. Pulsed output power versus current of one 1-cm-long GRIN-SCH-SQW laser bar of a hybrid two-dimensional surface-emitting array driven with 150-μsec pulses at repetition rates up to 500 Hz. The AlGaAs diode lasers were 40 μm wide on 125-μm centers.

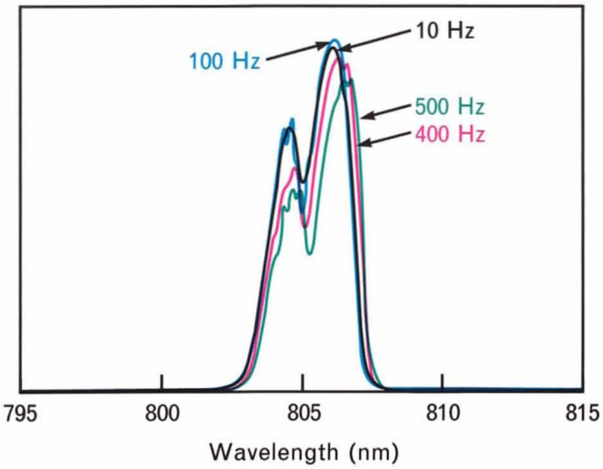

FIGURE 18. Output spectra of one 1-cm-long GRIN-SCH-SQW laser bar of a hybrid two-dimensional surface-emitting array driven with 30-A 150-μsec pulses at repetition rates of 10, 100, 400, and 500 Hz. The AlGaAs diode lasers were 40 μm wide on 125-μm centers.

per 1°C rise in temperature.) Figure 18 shows the output spectra of the bar driven with 150-μsec pulses of 30 A at repetition rates of 10, 100, 400, and 500 Hz. The additional temperature rise at the high repetition rates appears to be less than 1°C.

Figure 19 shows the L-I characteristics of a single bar for pulses ranging from 150 μsec to 1 msec at 10 Hz. The figure also shows the CW output for currents up to 25 A. Figure 20 contains a blow-up of the CW characteristics and the overall power efficiency η_p versus current. Note that the overall CW η_p at 25 A (including losses in the input wires that were not intended for CW operation) is 33%. For 150-μsec pulses, η_p (again including losses in the input wires) is ~38% at 40 A. We also measured the output spectra for 8-A 150-μsec pulses at 10 Hz and for 7- and 25-A CW operation. From that data, the estimated temperature rise for 25-A CW operation was ~30°C.

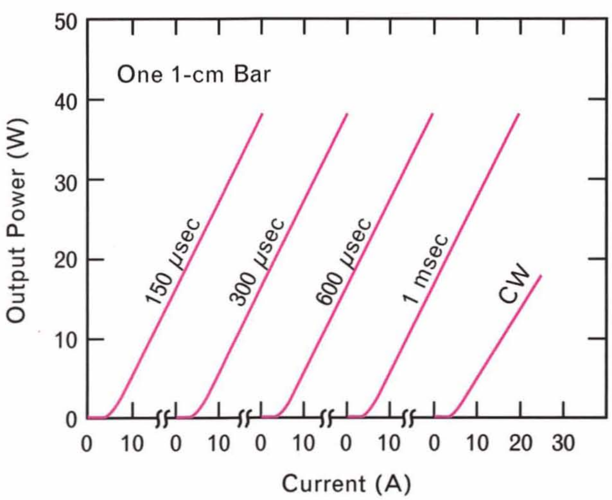

FIGURE 19. Output power versus current of one 1-cm-long GRIN-SCH-SQW laser bar of a hybrid two-dimensional surface-emitting array driven with 150-, 300-, and 600-μsec and 1-msec pulses at 10 Hz. Also shown is the CW output for current up to 25 A. The AlGaAs diode lasers were 40 μm wide on 125-μm centers.

We can use this value of temperature rise and an estimate of the power dissipated in the laser bar itself to obtain an estimate of the thermal resistance of the laser-bar/heat-sink combination. For 25-W CW operation, the total power into the laser bar (assuming each of the 80 lasers in the 1-cm bar has a series resistance of 0.2 Ω) is ~40 W. Thus, with an optical power output of 18 W, the dissipated power in the laser bar is ~22 W. With this dissipated power, the CW temperature rise of ~30°C gives a total effective thermal resistance of ~0.094°C-cm^2/W. This result is in close agreement with previous heat-sink measurements and calculations: from References 58 and 60, the thermal resistance is ~0.07°C-cm^2/W for the Si heat sink and ~0.02°C-cm^2/W for the 100-μm-thick laser bar.

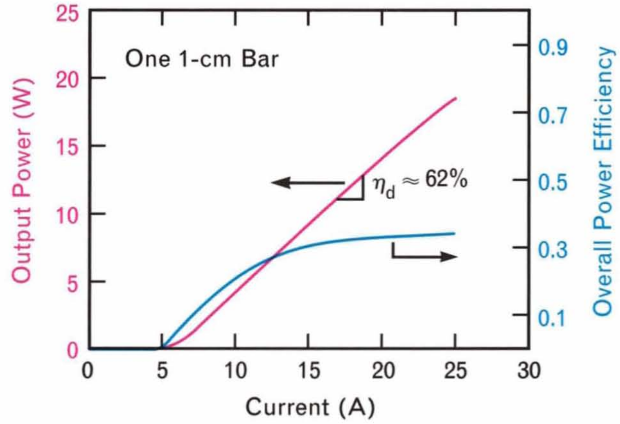

FIGURE 20. The CW output power and overall power efficiency versus current of one 1-cm-long GRIN-SCH-SQW laser bar of a hybrid two-dimensional surface-emitting array. The AlGaAs diode lasers were 40 μm wide on 125-μm centers.

After operating a bar in CW mode at 25 A for about 15 min, we measured the L-I characteristic of the bar driven with 150-μsec pulses at 10 Hz. The results indicated insignificant degradation (<5%) after the CW testing [50].

Figure 21 shows the CW output power versus current of six bars (0.75 cm^2) operating in parallel. Note that at 25 A per bar (a total current of 150 A), the output power is 90 W, or 120 W/cm^2, which is slightly less than the 144 W/cm^2 (18 W/bar × 8 bars/cm^2) obtained from the single-bar data of Figure 20.

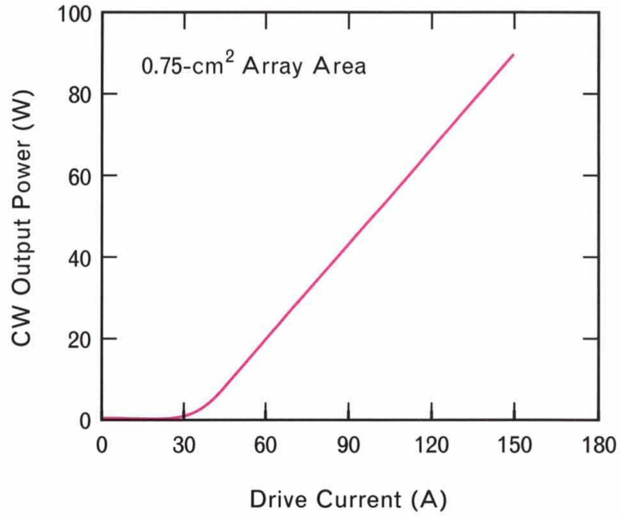

FIGURE 21. CW output power versus current of six 1-cm-long linear arrays (0.75-cm^2 area) of a hybrid microchannel-cooled module operated in parallel.

Monolithic Surface-Emitting Diode Laser Arrays

Although hybrid arrays have excellent performance characteristics, the fabrication and assembly of this type of laser require a great deal of skilled labor. Researchers are hopeful that monolithic arrays, which can be fabricated almost entirely with high-volume semiconductor processing techniques, will be more amenable to mass production. As a possible direct replacement for hybrid arrays, monolithic two-dimensional arrays of GaAs/AlGaAs diode lasers with light emission normal to the surface have been made by fabricating horizontal-cavity edge-emitting quantum-well lasers coupled with external mirrors that deflect the radiation from the laser facets by 90° (Figure 22[a]) [21, 23, 37, 38]. In addition, several preliminary surface-emitting arrays with intracavity 45° deflecting mirrors have been fabricated (Figures 22[b] and [c]) [21, 23]. In both types of arrays, ion-beam-assisted etching (IBAE) was used to form all the laser facets and deflecting mirrors.

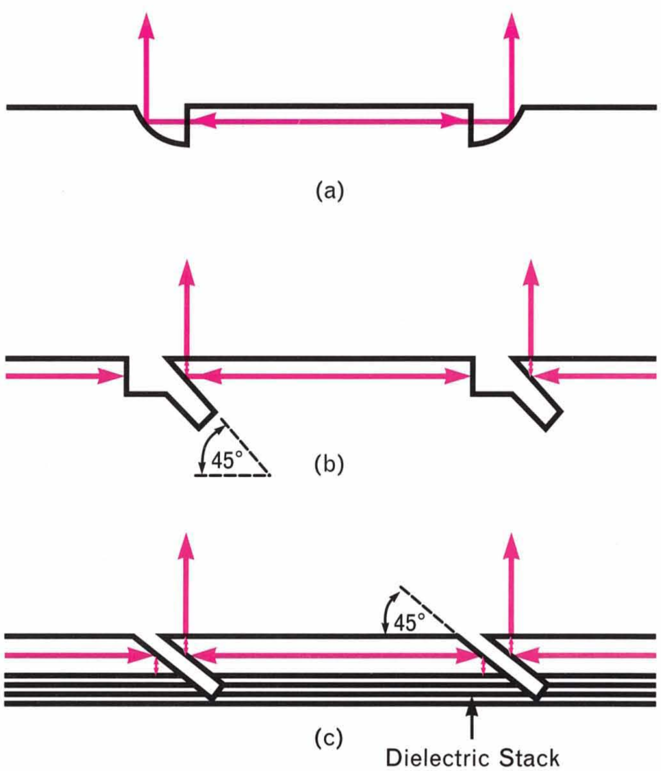

FIGURE 22. Geometries of three designs of monolithic surface-emitting lasers: (a) external-cavity parabolic deflector, (b) intracavity 45° mirror, and (c) intracavity 45° mirror with an internal dielectric mirror stack.

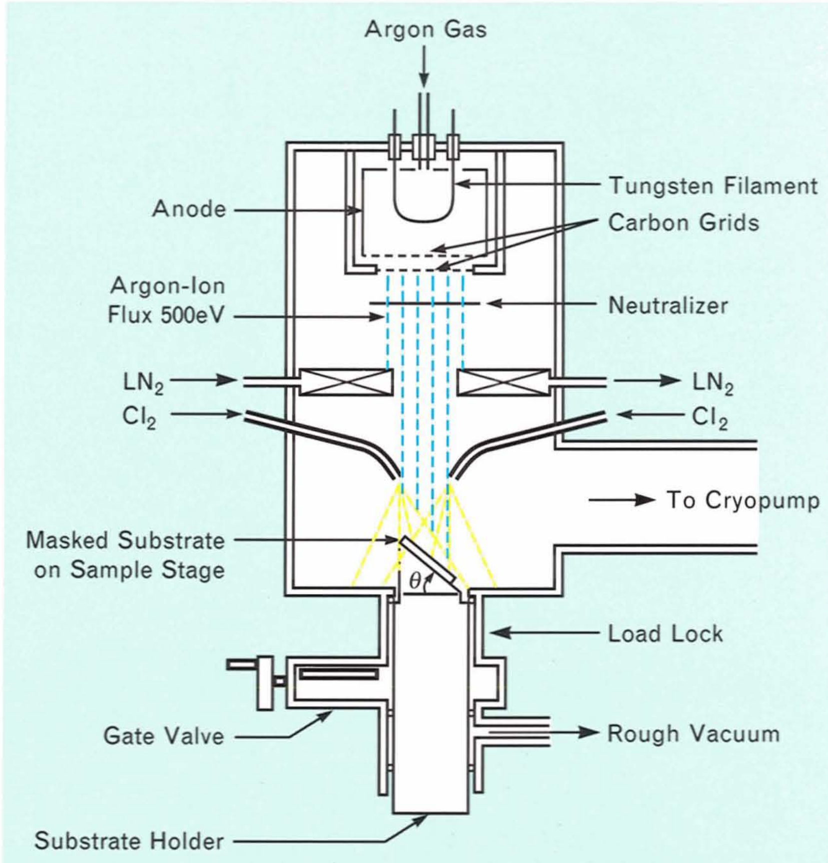

FIGURE 23. Schematic of Cl_2-ion-beam-assisted-etching (IBAE) system.

IBAE is a dry-etching technique in which the chemically reactant species and the energetic ions can be independently controlled. In Reference 42, Geis et al. describe the basic IBAE system. Figure 23 is a schematic illustration of an IBAE system with load lock, tiltable sample holder, and cryopump. In the system, which routinely reaches a background pressure of 10^{-7} Torr 15 min after sample loading, a chemically reactant species from a local jet and a separately controlled collimated ion beam from an ion source impinge simultaneously upon the sample. Both GaAs and AlGaAs can be etched at room temperature with Cl_2 as the reactant gas and argon as the source of ions. Because neither GaAs nor AlGaAs is spontaneously etched by Cl_2 at room temperature, IBAE is highly directional and the sidewall slope of a masked etch trench is determined essentially by the direction of the argon-ion beam. Therefore, almost any concave shape can be generated with a computer-controlled sample stage that precisely varies the tilt angle between the sample and the ion beam during etching [44]. Materials such as photoresist, phosphosilicate glass, SiO_2, Ni, and Ti that have slow etch rates compared to GaAs and AlGaAs can be used as etch masks.

For the work reported in this article, the system operating parameters were adjusted to give an etch rate of 120 nm/min at normal incidence for both GaAs and AlGaAs. The energy of the argon-ion beam was 500 eV and the current density was ~40 mA/cm^2. The pressure due to the argon-ion beam at the sample surface was 0.1 mTorr and the local chlorine pressure was 2.8 mTorr. With these parameters, we observed no roughness or steps at the GaAs/AlGaAs heterointerfaces.

Monolithic Arrays with External Deflecting Mirrors

We have fabricated monolithic two-dimensional surface-emitting arrays of GaAs diode lasers by using a combination of straight and angled IBAE to produce arrays of edge-emitting separate-confinement quantum-well lasers with deflecting mirrors adjacent to the laser facets (Figure 24). The AlGaAs/GaAs material used for these arrays was separate-confinement-heterostructure single-quantum-well (SCH-SQW) material that con-

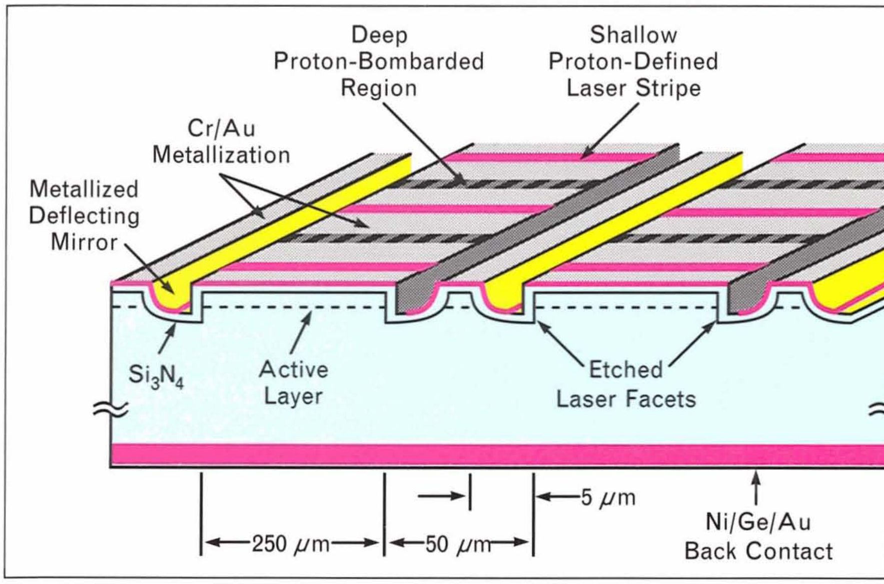

FIGURE 24. Schematic illustration of a monolithic two-dimensional surface-emitting array of GaAs/AlGaAs diode lasers with external parabolic deflecting mirrors.

tained an undoped 200-Å GaAs quantum well sandwiched between two 3200-Å-thick $Al_{0.3}Ga_{0.7}As$ confining layers, one n-type and the other p-type. The cladding layers contained 70 mole % AlAs. Cleaved-facet lasers fabricated from this SCH-SQW material had higher threshold current densities and lower differential quantum efficiencies ($\eta_d \cong 60\%$) than those of the GRIN-SCH-SQW material (Figure 3) now being used for the hybrid arrays. Because of the wide quantum-well thickness of the monolithic array lasers, however, the threshold current density does not increase as rapidly with decreasing cavity length. Nevertheless, longer cavity lengths than those used in the arrays reported in this article should result in better performance.

We used photoresist as an etch mask and IBAE to etch pairs of straight-sided grooves 2 μm wide and 3 to 4 μm deep. The outer walls of each pair acted as the facets for rows of laser cavities that were 250 μm long. Lines approximately 3 μm wide immediately adjacent to the inside edge of one of the grooves in each pair were then opened in a new layer of photoresist, and parabolic deflectors for one side of each row were formed by computer-controlled angled IBAE. The deflectors for the other side of each row were formed in a similar manner.

Figure 25 shows the near-field pattern of a 100-element two-dimensional surface-emitting array. A shallow proton bombardment was used to confine the current to 40-μm-wide stripes on 180-μm centers, and a deep proton bombardment midway between the laser stripes was used to introduce a sufficient optical loss to suppress transverse lasing. References 21 and 36 contain further details of the fabrication. Figure 26 plots the pulsed output power versus current for this array. The available pulsed current of 62 A limits the power to 15 W. Figure 27 plots the output power versus current for an array that consists of only two rows (a total of 20 elements) fabricated from the same wafer as that of Figure 26. The smaller array has a pulsed

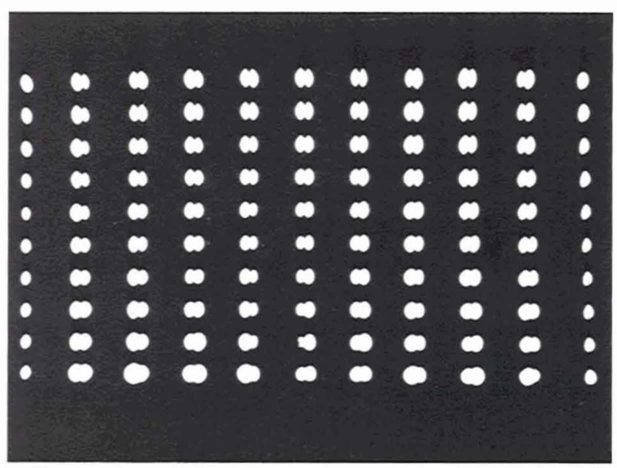

FIGURE 25. Near-field pattern of 100-element monolithic two-dimensional surface-emitting array of GaAs/AlGaAs diode lasers with external deflecting mirrors.

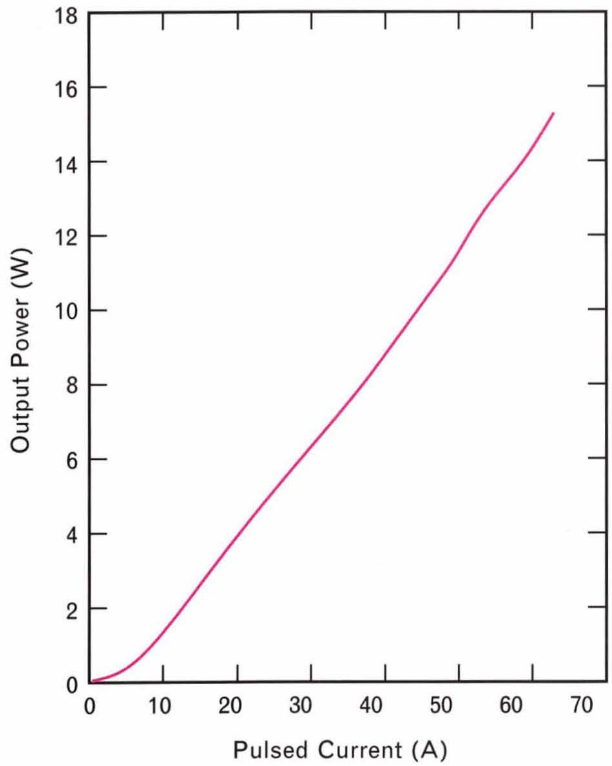

FIGURE 26. Pulsed output power versus current for the 100-element monolithic array whose near-field pattern is shown in Figure 25. The pulses are 500 nsec at 1 kHz and the area of the array is 5.4×10^{-2} cm^2.

power output of 16.5 W at 62 A, which corresponds to a power density of 1.5 kW/cm^2 [21, 23, 37, 38].

The differential quantum efficiency η_d of these arrays is about 20%. Several factors can limit η_d, including the quality of the laser facets, the beam divergence of the laser emission, and the effective f-number of the deflecting mirrors. The latter two factors affect the fraction of light emitted from the laser facets that is deflected by the deflecting mirrors. Although the quality of the laser facets can be a problem, the fraction deflected by the mirrors is currently the major limitation on η_d.

We can make several obvious changes to increase the fraction of light collected and to make this fraction less dependent on process variables. The first is to use laser material with a smaller output-beam divergence. Cleaved-facet lasers fabricated in the GRIN-SCH-SQW material now being used in the hybrid arrays have a beam divergence ≤36° (full width at half maximum), which is significantly smaller than the ≥45° measured in similar lasers fabricated in the SCH-SQW material used for the array whose near-field pattern is shown in Figure 25. (As mentioned previously, cleaved-facet lasers fabricated in the GRIN-SCH-SQW material also have a higher differential quantum efficiency [>80%].) In addition, making the junction slightly deeper (2.5 to 3 μm deep instead of 2 μm) and the facet etch narrower (1 to 1.5 μm wide instead of 2 μm) should increase the collection efficiency of the deflecting mirrors and make them more tolerant of photolithographic and etching inaccuracies.

With a planar top surface, curved deflectors are necessary to obtain an f-number less than 1. Figure 28 shows a design of an integral parabolic deflecting mirror with an f-number less than 0.85. The actual curve etched in the AlGaAs material is now being designed to optimize the f-number, with attention to the following factors: passivation and metal overlayers, the depth of the junction, and tolerances in the lithography used to form the etch mask. For the front surface of the deflector to be parabolic, etching a second-order polynomial curve is necessary.

Figure 29(a) illustrates the method [23] that we are now using to etch the curve in the laser material. First the curve is broken down into a number of line seg-

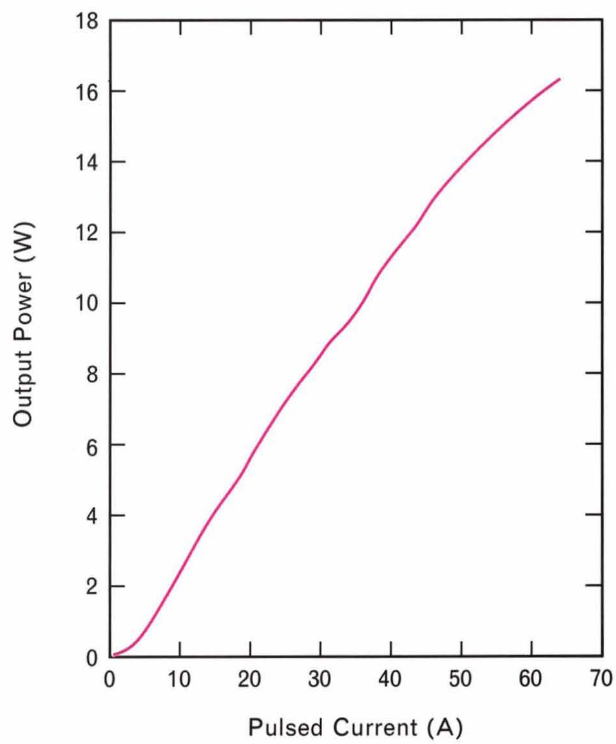

FIGURE 27. Pulsed output power versus current for a 20-element (two rows of 10 elements) two-dimensional array of GaAs/AlGaAs diode lasers. The pulses are 500 nsec at 1 kHz and the array area is 1.08×10^{-2} cm^2.

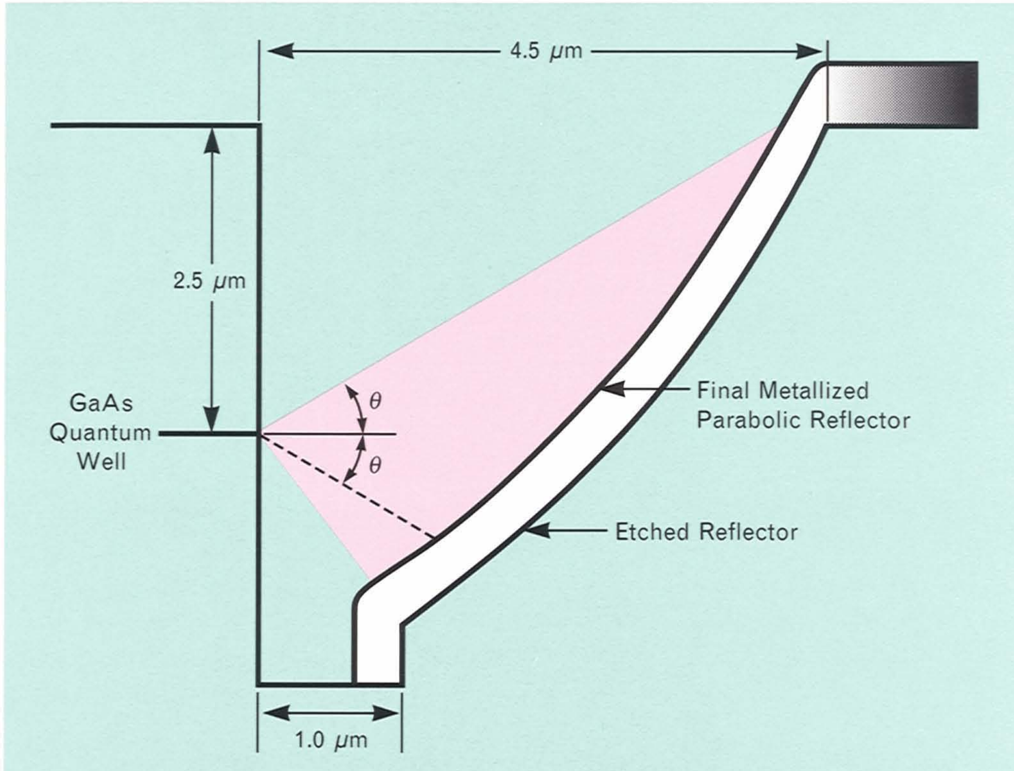

FIGURE 28. Illustration of an external deflecting mirror. The effective f-number is less than 0.85 and the minimum θ is 30.5°.

ments of length L_n, which is determined by the resolution of the computer-controlled stepping motor. Once the daily etch rate is determined, the time required to etch each segment t_n is calculated from the formula $t_n = L_n/(r \cos \phi_n)$, where r is the etch rate and ϕ_n is the incident angle of the argon-ion beam. The resolution of the steps coupled with the slight divergence of the ion beam (~0.5°) create a smooth surface with the individual etched segments blended together. Figure 29(b) compares the desired theoretical curve with an actual etched curve. Note the excellent agreement between the two curves; the small amount of deviation is most likely due to an error in determining the etch rate. To achieve even greater accuracy, we are currently determining the rate by using a surface-profile technique in place of optical microscopy.

The scanning-electron micrographs in Figure 30 show the face of a typical etched facet and the surface of a typical etched deflector. We found that a photoresist mask did not hold up well during the vertical-facet formation but was sufficient for etching the deflectors because the tilting action in the latter procedure shifted the edge of the mask and minimized the mask-edge erosion. We are now using a silicon-dioxide mask for etching and a self-aligning process for accurately fixing the facet-to-deflector distance. With these changes, it should be possible to fabricate parabolic deflecting mirrors with effective f-numbers less than one and arrays with $\eta_d > 60\%$.

Monolithic Arrays with Intracavity Deflecting Mirrors

Using a combination of straight and 45° IBAE, we have fabricated monolithic two-dimensional surface-emitting arrays with intracavity 45° mirrors (Figure 31) [21, 23]. Lasers of this type are sometimes called folded-cavity lasers [22, 23]. We etched the arrays in one photolithography step. With photoresist as an etch mask, we used IBAE to etch straight-sided grooves 6 μm wide. Without removing the sample from the etch chamber, we tilted the sample at a 45° angle and etched the 45° intracavity mirrors. Figure 32, an optical micrograph of a cleaved cross section of an IBAE test sample, shows the success of the technique. Some erosion of the photoresist etch mask occurred, which produced steps in the vertical facet and 45° mirror. The step in the vertical facet, however, was above the laser active layer and the

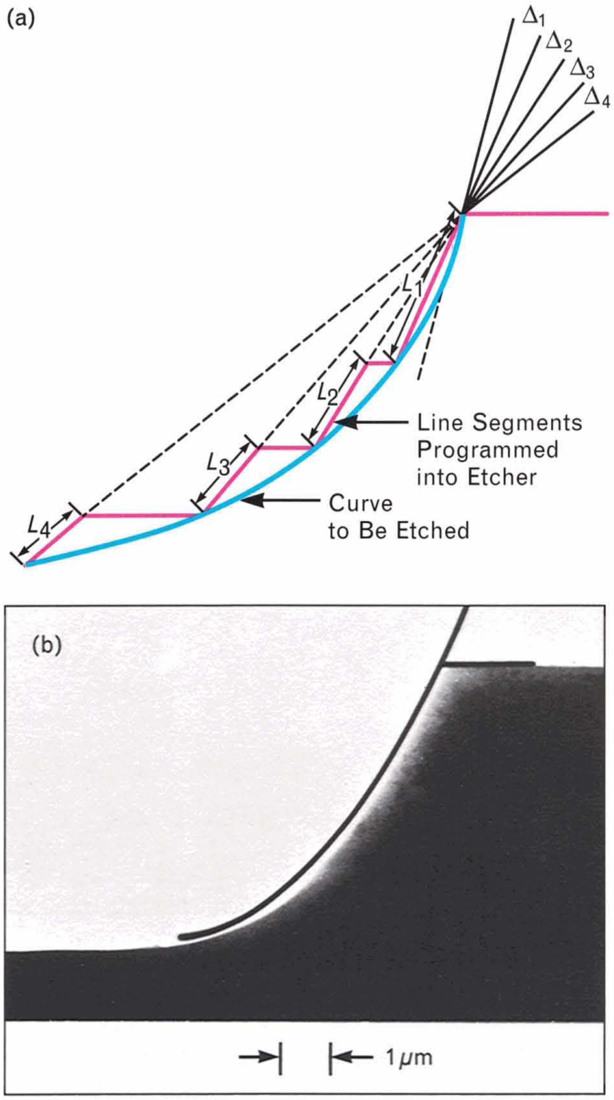

FIGURE 29. (a) Dynamic tilting algorithm employed in micromachining the polynomial curve required to produce a parabolic deflector. The quantity Δ_n is the angular displacement generated by a step of the motor, and L_n is the segment length at each step. (b) Optical micrograph of a cleaved cross section of a parabolic deflector. The black curved line represents the desired theoretical curve.

step in the 45° mirror was below the active layer. Thus their effect on device performance was not catastrophic.

Figure 33 shows the near-field pattern of a 100-element array. Note the one bad element in the fourth row and the scattering in the fifth row. All of the other lasers were operational. Figure 34 shows the pulsed output power versus current for the first row of the array (a total of 20 elements). The average threshold current is high, about 1 A per laser, and the differential quantum efficiency is low, about 4%. One factor that degraded the performance of this first array was the optical loss in the p+-GaAs capping layer, which was not removed from the window region.

Obviously, more work is needed to improve the quality and accuracy of both the 45° etch and the vertical etch in this device. Other parameters that could potentially limit the performance of the device are the parallelism and quality of the top surface facet, the diffraction between the top facet and the 45° mirror, and the absorption in any GaAs contacting layer left on the surface of the wafer. We expect the use of a silicon-

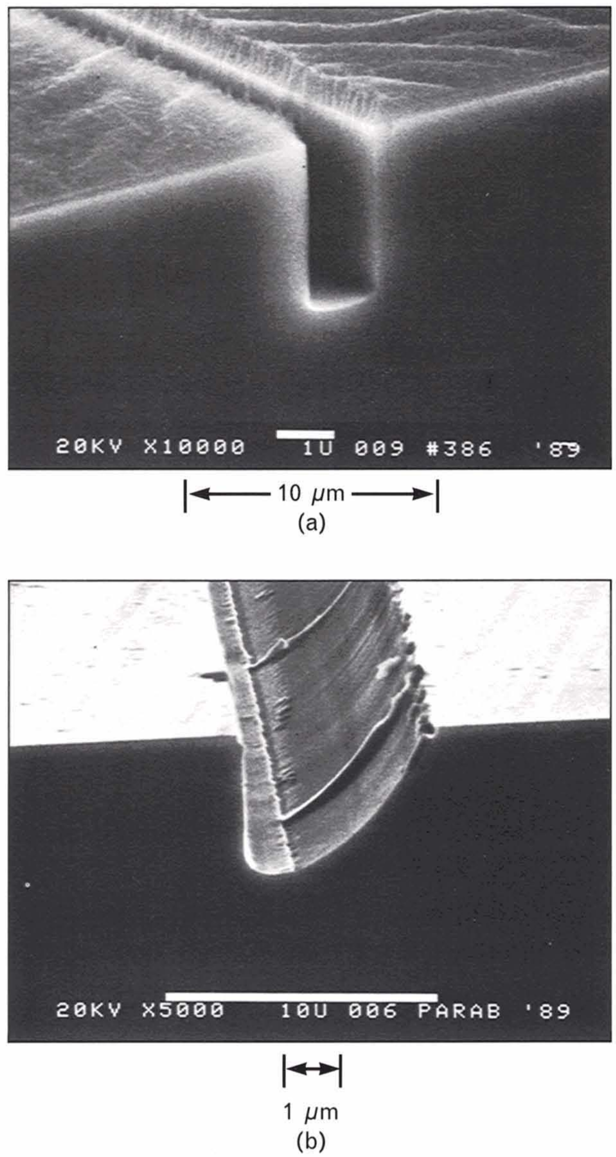

FIGURE 30. Scanning-electron micrographs of (a) the face of an etched vertical facet and (b) the etched surface of a parabolic deflector.

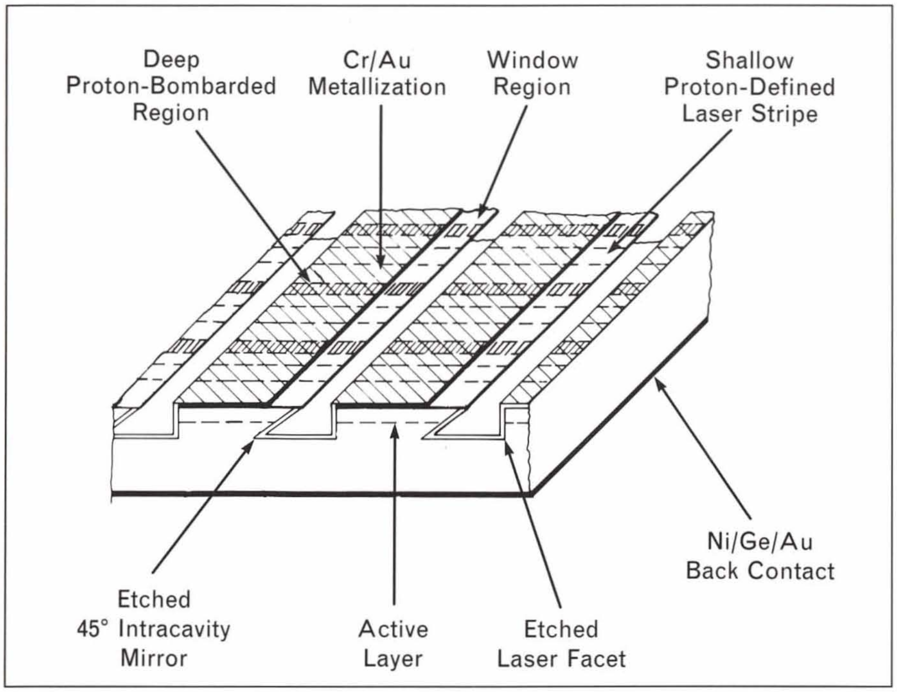

FIGURE 31. Schematic illustration of a monolithic two-dimensional surface-emitting array of GaAs/AlGaAs diode lasers with intracavity 45° deflecting mirrors.

dioxide or metal etch mask to improve the quality of the surfaces dramatically, which would in turn improve array performance. In addition, future arrays will be fabricated with the capping layer removed.

We have also fabricated monolithic arrays that had two internal 45° mirrors and an integral high-reflectivity dielectric mirror stack (Figure 22[c]) [23]. For this type of array, forming the internal and top-surface facets in one step minimized the IBAE and processing time. The dielectric mirror stack, which consisted of 20 pairs of alternating layers of $Al_{0.2}Ga_{0.8}As$ and $Al_{0.8}Ga_{0.2}As$, had a reflectivity of ~95% at the lasing wavelength of interest. The arrays performed similarly to the internal-cavity 45° mirror arrays that had one etched 90° facet.

In addition to the problems associated with arrays that have one etched 90° facet, diffraction and series resistance in the dielectric mirror stack must be considered for the arrays that have two internal 45° mirrors. As discussed earlier, better-quality 45° mirrors and the removal of the p^+-GaAs capping layer should improve the performance of this type of laser.

Summary

Several approaches to fabricating two-dimensional surface-emitting arrays of GaAs/AlGaAs diode lasers are being developed at Lincoln Laboratory.

Modules of hybrid diode laser arrays that utilize linear laser arrays with cleaved facets and microchannel Si heat sinks with integral 45° deflecting mirrors have been

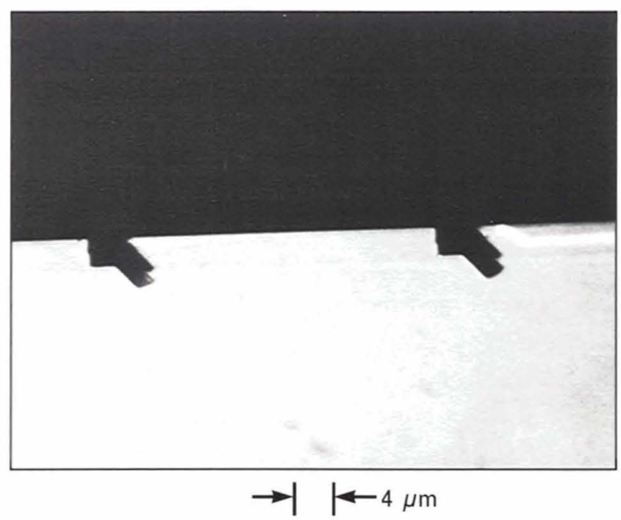

FIGURE 32. Optical micrograph of the cleaved cross section of a test wafer, profiling the vertical facet and 45°-mirror structure of the intracavity 45° deflecting mirror, or folded-cavity, design. After the vertical facet is formed, the sample is tilted in situ and the 45° mirror is etched.

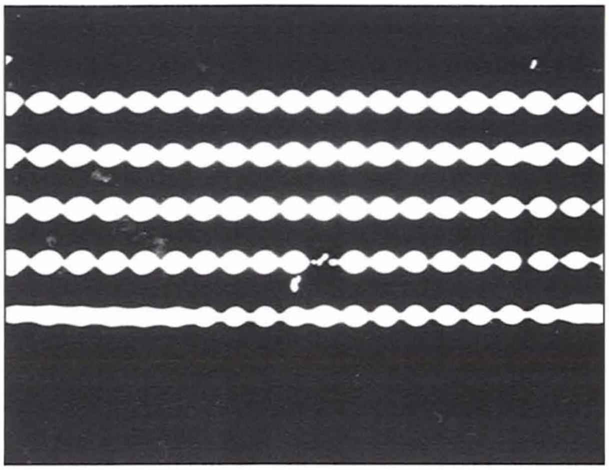

FIGURE 33. Near-field pattern of 100-element monolithic two-dimensional surface-emitting array of GaAs/AlGaAs diode lasers with intracavity 45° deflecting mirrors.

fabricated and tested. The modules, each containing two 1-cm^2 hybrid arrays, can be stacked and are designed to pump Nd:YAG slab lasers. For quasi-CW operation (150-μsec pulses), test data indicate that the modules can achieve peak output powers greater than 400 W/cm^2 (800 W/module, or 120 mJ per pulse per module) at repetition rates up to 500 Hz. The data also indicate that CW output powers of 120 to 150 W/cm^2 can be achieved.

In addition to the hybrid design, two monolithic approaches are being investigated. The first incorporates edge-emitting lasers with external-cavity deflecting mirrors adjacent to the laser facets. Using ion-beam-assisted etching (IBAE) to etch both the laser facets and deflecting mirrors, we fabricated 100-element arrays capable of short-pulsed (500 nsec) output powers greater than 1 kW/cm^2. The quantum efficiencies of the arrays are low, however, and further development is needed before this type of monolithic array will have performance characteristics comparable to the hybrid arrays. The monolithic arrays, however, should be more amenable to mass production, and consequently they hold the promise of lower cost. In addition, since the laser spacing is set photolithographically in both directions, it should be easier to combine this type of array with arrays of lenses for higher intensities, which could be exploited for the side-pumping or end-pumping of Nd:YAG lasers, or for the coherent locking of the individual lasers of the arrays in an external cavity.

The second monolithic approach incorporates intracavity 45° deflecting mirrors. Preliminary results on such monolithic arrays indicate that the threshold currents and differential quantum efficiencies are poor compared to the arrays of external-cavity deflecting mirrors. However, the intracavity-mirror arrays would have some advantages over the external-cavity-mirror arrays in some applications. The intracavity-mirror arrays are also easier to fabricate, and they therefore merit further investigation.

Acknowledgments

The author gratefully acknowledges his collaborators, who actually were the ones responsible for most of the work reported in this article: R.J. Bailey, for his ingenuity in device fabrication and packaging; K. Rauschenbach, for his fortitude in developing much of the unglamorous technology needed for the hybrid arrays and for his many contributions to the monolithic-array program; W.D. Goodhue, who brought ion-beam-assisted etch-

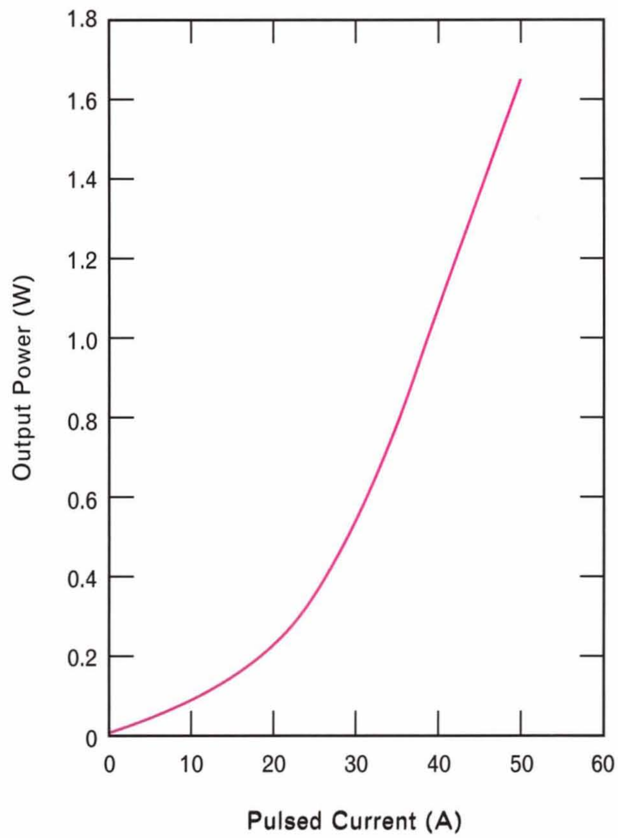

FIGURE 34. Pulsed output power versus current for one row (20 elements) of the array whose near-field pattern is shown in Figure 33. The pulses are 500 nsec at 1 kHz.

ing to the fabrication of monolithic arrays; C.A. Wang, for her unique talent and perseverance in developing the epitaxial technology necessary to grow the high-quality laser material used in this work and for not quitting when she was told the program needed "only" 40 more wafers; J.N. Walpole, for his insights into semiconductor diode lasers and microchannel heat sinks and for his numerical heat-flow calculations; L.J. Missaggia, for his many contributions to this program, especially his expertise in heat-sink-module design and assembly; J.D. Woodhouse, for supervising the fabrication of the linear arrays; V. Diadiuk, for her unselfish effort in producing the microchannel Si heat sinks; and V. Daneu, for his independent measurements on the hybrid arrays. The author would also like to acknowledge H.K. Choi, F.J. O'Donnell, G.A. Ferrante, G.D. Johnson, D.B. Hoyt, and C.D. Hoyt for their many contributions to this project, and S.M. McNeill, P.S. Day, M.D. McAleese, and D.M. Tracy for their technical assistance. The continued interest of R.C. Williamson, D.L. Spears, A. Sanchez-Rubio, and I. Melngailis is also greatly appreciated.

This work was sponsored by the Department of the Navy for SDIO and the Department of the Air Force.

REFERENCES

1. G.L. Harnagel, P.S. Cross, C.R. Lennon, M. Devito, and D.R. Scifres, "Ultra-High-Power Quasi-CW Monolithic Laser Diode Array with High Power Conversion Efficiency," *Electron. Lett.* **23**, 743 (1987).
2. D.F. Welch, W. Streifer, B. Chan, and D.R. Scifres, "High-Power, 8 W CW, Single-Quantum-Well Laser Diode Arrays," *Electron. Lett.* **24**, 113 (1988).
3. M. Sakamoto, D.F. Welch, G.L. Harnagel, W. Streifer, H. Kung, and D.R. Scifres, "Ultra-High-Power 38 W Continuous-Wave Monolithic Laser Diode Arrays," *Appl. Phys. Lett.* **52**, 2220 (1988).
4. M. Sakamoto, D.F. Welch, T.G. Erdriz, D.R. Scifres, and W. Streifer, "76 W CW Monolithic Laser Diode Arrays," *Appl. Phys. Lett.* **54**, 2299 (1989).
5. L.J. Mawst, D. Botez, M. Jansen, T.J. Roth, and G. Peterson, "High-Power, Narrow Single-Lobe Operation from 20-Element Phase-Locked Array of Antiguides," *Appl. Phys. Lett.* **55**, 2060 (1989).
6. M. Jansen, J.J. Yang, S.S. Ou, D. Botez, J. Wilcox, and L. Mawst, "Diffraction-Limited Operation from Monolithically Integrated Diode Laser Array and Self-Imaging (Talbot) Cavity," *Appl. Phys. Lett.* **55**, 1949 (1989).
7. P.S. Cross, G.L. Harnagel, W. Streifer, D.R. Scifres, and D.F. Welch, "Ultrahigh-Power Semiconductor Diode Laser Arrays," *Science* **237**, 1305 (1987).
8. W. Streifer, D.R. Scifres, G.L. Harnagel, D.F. Welch, J. Berger, and M. Sakamoto, "Advances in Diode Laser Pumps," *IEEE J. Quantum Electron.* **24**, 883 (1988).
9. C.A. Krebs and B.D. Vivian, "High Power Quasi-CW and CW Laser Diode Bar Arrays," *SPIE* **893**, 35 (1988).
10. A. Rosenberg, J.C. McShea, A.R. Bogdan, J.C. Petheram, A. Rosen, D. Bechtle, P.S. Zory, J.W. Sprague, and J.R. Shealy, "High-Power, High-Efficiency 770 nm 2D Laser Diode Array," *Electron. Lett.* **24**, 1121 (1988).
11. A. Rosen, P. Stabile, W. Janton, J.C. McShea, A. Rosenberg, J.C. Petheram, H.G. Miller, J.W. Sprague, and J.M. Gilman, "1 kw Peak Power 808 nm 2-D Laser Diode Array," *IEEE Photonics Technol. Lett.* **1**, 43 (1989).
12. K. Iga, F. Kayama, and S. Kinoshita, "Surface Emitting Semiconductor Lasers," *IEEE J. Quantum Electron.* **QE-24**, 1845 (1988).
13. M.Y.A. Raja, S.R.J. Brueck, M. Osiński, C.F. Schaus, J.G. McInerney, T.M. Brennan, and B.E. Hammons, "Resonant Periodic Gain Surface-Emitting Semiconductor Lasers," *IEEE J. Quantum Electron.* **25**, 1500 (1989).
14. S.W. Corzine, R.S. Geels, J.W. Scott, R.-H. Yan, and L.A. Coldren, "Design of Fabry-Perot Surface-Emitting Lasers with a Periodic Gain Structure," *IEEE J. Quantum. Electron.* **25**, 1513 (1989).
15. L.M. Zinkiewicz, T.J. Roth, L.J. Mawst, D. Tran, and D. Botez, "High Power Vertical-Cavity Surface-Emitting AlGaAs/GaAs Diode Lasers," *Appl. Phys. Lett.* **54**, 1959 (1989).
16. D. Botez, L.M. Zinkiewicz, T.J. Roth, L.J. Mawst, and G. Peterson, "Low-Threshold-Current-Density Vertical-Cavity Surface-Emitting AlGaAs/GaAs Diode Lasers," *IEEE Photonics Technol. Lett.* **1**, 205 (1989).
17. J.L. Jewell, K.F. Huang, K. Tai, Y.H. Lee, R.J. Fischer, S.L. McCall, and A.Y. Cho, "Vertical Cavity Single Quantum Well Lasers," *Appl. Phys. Lett.* **55**, 424 (1989).
18. A.J. SpringThorpe, "A Novel Double-Heterostructure *p-n* Junction Laser," *Appl. Phys. Lett.* **31**, 524 (1977).
19. T. Yuasa, N. Hamao, M. Sugimoto, N. Takado, M. Ueno, H. Iwata, Y. Tashiro, K. Onabe, and K. Asakawa, "Surface-Emitting GaAs/AlGaAs Multi-Quantum Well Lasers with Optical Bistability," *Conf. Lasers Electro-Optics Tech. Dig. 1988* **7**, 258 (1988).
20. N. Hamao, M. Sugimoto, N. Takado, Y. Tashiro, H. Iwata, T. Yuasa, and K. Asakawa, "Surface-Emitting GaAs/AlGaAs Lasers with Dry-Etched 45° Total Reflecting Mirrors," *Appl. Phys. Lett.* **54**, 2389 (1989).
21. J.P. Donnelly, K. Rauschenbach, C.A. Wang, W.D. Goodhue, and R.J. Bailey, "Two-Dimensional Surface-Emitting Arrays of GaAs/AlGaAs Diode Lasers," *Proc. SPIE* **1043**, 92 (1989).
22. T. Takamori, L.A. Coldren, and J.L. Merz, "Folded-Cavity Transverse Junction Stripe Surface-Emitting Laser," *Appl. Phys. Lett.* **55**, 1053 (1989).
23. W.D. Goodhue, K. Rauschenbach, C.A. Wang, J.P. Donnelly, R.J. Bailey, and G.D. Johnson, "Monolithic Two-Dimensional GaAs/AlGaAs Laser Arrays Fabricated by Chlorine Ion-Beam Assisted Etching," *J. Electron. Mater.* **19**, 463 (1990).
24. S.S. Ou, M. Jansen, J.J. Yang, and M. Sergant, "High Performance GaAs/AlGaAs Edge-Emitting and Surface-Emitting Lasers with Reliable Dry Etched Facets," presented as post-deadline paper at CLEO '90, Anaheim, CA, CPDP31.
25. Z.L. Liau, J.N. Walpole, L.J. Missaggia, and D.E. Mull, "GaInAsP/InP Buried-Heterostructure Surface Emitting Diode Laser with Monolithic Integrated Bifocal Microlens," *Appl. Phys. Lett.* **56**, 1219 (1990).
26. G.A. Evans, N.W. Carlson, J.M. Hammer, M. Lurie, J.K.

Butler, S.L. Palfrey, R. Amantea, L.A Carr, F.Z. Hawrylo, E.A. James, C.J. Kaiser, J.B. Kirk, and W.F. Reichert, "Two-Dimensional Coherent Laser Arrays Using Grating Surface Emission," *IEEE J. Quantum. Electron.* **25,** 1525 (1989).

27. G.A. Evans, N.W. Carlson, J.M. Hammer, M. Lurie, J.K. Butler, L.A. Carr, F.Z. Hawrylo, E.A. James, C.J. Kaiser, J.B. Kirk, W.F. Reichert, S.R. Chinn, J.R. Sheahy, and P.S. Zory, "Efficient, High-Power (>150 mW) Grating Surface Emitting Lasers" *Appl. Phys. Lett.* **52,** 1037 (1988).
28. J.S. Mott and S.H. Macomber, "Two-Dimensional Surface Emitting Distributed Feedback Laser Arrays," *IEEE Photonics Technol. Lett.* **1,** 202 (1989).
29. R. Parke, R. Waarts, D.F. Welch, A. Hardy, and W. Streifer, "High Efficiency, High Uniformity Grating Coupled Surface-Emitting Lasers," *Electron. Lett.* **26,** 125 (1990).
30. R.L. Thornton, R.D. Burnham, and W. Streifer, "High Reflectivity GaAs-AlGaAs Mirrors Fabricated by Metalorganic Chemical Vapor Deposition," *Appl. Phys. Lett.* **45,** 1028 (1984).
31. Z.L. Liau and J.N. Walpole, "Mass-Transported GaInAsP/InP Lasers," *Lincoln Laboratory J.* **2,** 77 (1989).
32. J.A. Walpole and Z.L. Liau, "Monolithic Two-Dimensional Arrays of High-Power GaInAsP/InP Surface-Emitting Diode Lasers," *Appl. Phys. Lett.* **48,** 1636 (1986).
33. Z.L. Liau and J.N. Walpole, "Large Monolithic Two-Dimensional Arrays of GaInAsP/InP Surface-Emitting Lasers," *Appl. Phys. Lett.* **50,** 528 (1987).
34. T.H. Windhorn and W.D. Goodhue, "Monolithic GaAs/AlGaAs Diode Laser/Deflector Devices for Light Emission Normal to the Surface," *Appl. Phys. Lett.* **48,** 1675 (1986).
35. J.J. Yang, M. Jansen, and M. Sergant, "Surface-Emitting GaAlAs/GaAs Laser with Etched Mirrors," *Electron. Lett.* **22,** 438 (1986).
36. J.J. Yang, M. Sergant, M. Jansen, S.S. Ou, L. Eaton, and W.W. Simmons, "Surface-Emitting GaAlAs/GaAs Linear Laser Arrays with Etched Mirrors," *Appl. Phys. Lett.* **49,** 1138 (1986).
37. J.P. Donnelly, W.D. Goodhue, T.H. Windhorn, R.J. Bailey, and S.A. Lambert, "Monolithic Two-Dimensional Surface-Emitting Arrays of GaAs/AlGaAs Diode Lasers," *Appl. Phys. Lett.* **51,** 1138 (1987).
38. J.P. Donnelly, K.K. Anderson, J.D. Woodhouse, W.D. Goodhue, D. Yap, M.C. Gaidis, and C.A. Wang, "Some Applications of Ion Beams in III-V Compound Semiconductor Device Fabrication," in *Advances in Materials, Processing and Devices in III-V Semiconductors,* eds. D.K. Sadana, L.E. Eastman, and R. Dupuis, *Mat. Res. Soc. Proc.* **144,** 421 (1988).
39. M. Jansen, J.J. Yang, L. Heflinger, S.S. Ou, M. Sergant, J. Huang, J. Wilcox, L. Eaton, and W. Simmons, "Coherent Operation of Injection-Locked Monolithic Surface-Emitting Diode Laser Array," *Appl. Phys. Lett.* **54,** 2634 (1989).
40. Z.L. Liau, J.N. Walpole, and D.Z. Tsang, "Fabrication, Characterization, and Analysis of Mass-Transported GaInAsP/InP Buried-Heterostructure Lasers," *IEEE J. Quantum Electron.* **QE-20,** 855 (1984).
41 Z.L. Liau, J.N. Walpole, and D.Z. Tsang, "Low-Threshold GaInAsP/InP Buried-Heterostructure Lasers with Chemically Etched and Mass-Transported Mirror," *Appl. Phys. Lett.* **44,** 945 (1984).
42. M.W. Geis, G.A. Lincoln, N. Efremow, and W.J. Piacentini, "A Novel Anisotropic Dry Etching Technique," *J. Vac. Sci. Technol.* **19,** 1390 (1981).
43. G.A. Lincoln, M.W. Geis, S. Pang, and N.N. Efremow, "Large Area Ion Beam Assisted Etching of GaAs with High Etch Rates and Controlled Anisotropy," *J. Vac. Sci. Technol.* **B1,** 1043 (1983).
44. W.D. Goodhue, G.D. Johnson, and T.H. Windhorn, "Angular Chlorine Ion-Beam-Assisted Etching of GaAs and AlGaAs," in *Gallium Arsenide and Related Compounds 1986,* ed. W.T. Lindley (IOP Publishing, Bristol, UK, 1987), p. 349.
45. N. Takado, K. Asakawa, T. Yuasa, S. Sugata, E. Miyauchi, H. Hashimoto, and M. Ishii, "Chemically Enhanced Focused Ion Beam Etching of Deep Grooves and Laser-Mirror Facets in GaAs under Cl_2 Gas Irradiation Using a Fine Nozzle," *Appl. Phys. Lett.* **50,** 1891 (1987).
46. P. Tihanyi, D.K. Wagner, A.J. Roza, H.J. Vollmer, C.M. Harding, R.J. Davis, and E.D. Wolf, "High-Power AlGaAs/GaAs Single Quantum Well Lasers with Chemically Assisted Ion Beam Etched Mirrors," *Appl. Phys. Lett.* **50,** 1640 (1987).
47. J.A. Skidmore, L.A. Coldren, E.L. Hu, J.L. Merz, and K. Asakawa, "Use of Independently Controlled Cl Radical and Ar Ion Beams for Anisotropic Chemically Enhanced Etching of GaAs," *Appl. Phys. Lett.* **53,** 2308 (1988).
48. T. Takamori, L.A. Coldren, and J.L. Merz, "Angled Etching of GaAs/AlGaAs by Conventional Cl_2 Reactive Ion Etching," *Appl. Phys. Lett.* **53,** 2549 (1988).
49. J.P. Donnelly, R.J. Bailey, C.A. Wang, G.A. Simpson, and K. Rauschenbach, "Hybrid Approach to Two-Dimensional Surface-Emitting Diode Laser Arrays," *Appl. Phys. Lett.* **53,** 938 (1988).
50. J.P. Donnelly, K. Rauschenbach, C.A. Wang, R.J. Bailey, J.N. Walpole, L.J. Missaggia, J.D. Woodhouse, H.K. Choi, F.J. O'Donnell, and V. Diadiuk, "High-Power Hybrid Two-Dimensional Surface-Emitting AlGaAs Diode Laser Arrays," *Proc. SPIE* **1219,** 255 (1990).
51. J.R. Leger, M.L. Scott, and W.B. Veldkamp, "Coherent Addition of AlGaAs Lasers Using Microlenses and Diffractive Coupling," *Appl. Phys. Lett.* **52,** 1771 (1988).
52. V. Diadiuk, Z.L. Liau, J.N. Walpole, J.W. Caunt, and R.C. Williamson, "External-Cavity Coherent Operation of InGaAsP Buried-Heterostructure Laser Array," *Appl. Phys. Lett.* **55,** 2161 (1989).
53. D.B. Tuckerman and R.F.W. Pease, "High-Performance Heat Sinking for VLSI," *IEEE Electron Device Lett.* **2,** 126 (1981).
54. S. Sasaki and T. Kishimoto, "Optimal Structure for Microgrooved Cooling Fin for High-Power LSI Devices," *Electron. Lett.* **22,** 1332 (1986).
55. R.J. Phillips, "Forced-Convection, Liquid-Cooled Microchannel Heat Sinks," M.S. thesis, Dept. of Mechanical Engineering, MIT, Cambridge, MA (1987). (Also NTIS, AD-A-193-337, ESD-TR-87-023, 1988).
56. R.J. Phillips, L.R. Glicksman, and R. Larson; "Forced-Convection, Liquid-Cooled, Microchannel Heat Sinks for High-Power-Density Microelectronics," in *Cooling Technology for Electronic Equipment,* ed. W. Aung (Hemisphere Publishing Corp., New York, 1988), p. 295.
57. R.J. Phillips, "Microchannel Heat Sinks," *Lincoln Laboratory J.* **1,** 31; errata, p. 258 (1988).
58. J.N. Walpole, Z.L. Liau, V. Diadiuk, and L.J. Missaggia, "Microchannel Heat Sinks and Microlens Arrays for High Average-Power Diode Laser Arrays," presented at IEEE Laser and Electro-Optic Society 1988 LEOS Annual Meeting, 2–4 Nov. 1988, Santa Clara, paper ThW.4.
59. D. Mundinger, R. Beach, W. Benett, R. Solarz, W. Krupke, R. Stavan, and D. Tuckerman, "Demonstration of High-Performance Silicon Microchannel Heat Exchangers for Laser Diode Array Cooling," *Appl. Phys. Lett.* **53,** 1030 (1988).
60. L.J. Missaggia, J.N. Walpole, Z.L. Liau, and R.J. Phillips, "Microchannel Heat Sinks for Two-Dimensional High-Pow-

er-Density Diode Laser Arrays," *IEEE J. Quantum Electron.* **25,** 1988 (1989).
61. C.A. Wang, H.K. Choi, and M.K. Connors, "Highly Uniform GaAs/AlGaAs GRIN-SCH-SQW Diode Lasers Grown by Organometallic Vapor Phase Epitaxy," *IEEE Photonics Technol. Lett.* **1,** 351 (1989).
62. C.A. Wang, "A New Organometallic Vapor Phase Epitaxy Reactor for Highly Uniform Epitaxy," *Lincoln Laboratory J.* **3,** 3 (1990).
63. W.G. Oldham and A.G. Milnes, "n-n Semiconductor Heterojunctions," *Solid-State Electron.* **6,** 121 (1963).
64. D.T. Cheung, S.Y. Chiang, and G.L. Pearson, "A Simplified Model for Graded-Gap Heterojunctions," *Solid-State Electron.* **18,** 263 (1975).
65. A.G. Foyt, W.T. Lindley, C.M. Wolfe, and J.P. Donnelly, "Isolation of Junction Devices in GaAs Using Proton Bombardment" *Solid-State Electron.* **12,** 209 (1969).
66. J.C. Dyment, J.C. North, and L.A. D'Asaro, "Optical and Electrical Properties of Proton-Bombardment," *J. Appl. Phys.* **44,** 207 (1973).
67. J.N. Walpole, private communication.
68. V. Daneu, private communication.

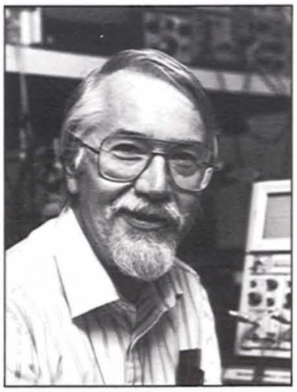

JOSEPH P. DONNELLY was born in Brooklyn, N.Y., in 1939. He received a B.E.E. degree from Manhattan College, Bronx, N.Y., in 1961 and M.S. and Ph.D. degrees in electrical engineering from Carnegie Institute of Technology (now Carnegie-Mellon University), Pittsburgh, Pa., in 1962 and 1966, respectively.

From 1965 to 1966 he was NATO Post-Doctoral Fellow at Imperial College, London. In 1967 he joined Lincoln Laboratory, where he is currently a staff member in the Applied Physics Group. His work at Lincoln Laboratory has included the development of compound-semiconductor ion-implantation technology and a variety of compound-semiconductor electronic and eletro-optical devices. His current interests include the experimental and theoretical aspects of integrated guided-wave optical devices, two-dimensional laser diode arrays, and high-power millimeter-wave devices.

Joe was a National Lecturer for the IEEE Electron Devices Society in 1979 and is the author or coauthor of two book chapters and more than 100 journal articles. He is a Fellow of the IEEE, a member of The Bohmesche Physical Society and Eta Kappa Nu, and an associate member of Sigma Xi.